Distinguishing Desirable and Undesirable Reactions in Multicomponent Systems for Redox Activation of the Uranyl Ion

Emily R. Mikeska,[a] Małgorzata Z. Makoś,[b] Grant A. Arehart,[a] Vassiliki-Alexandra Glezakou,[b,] and James D. Blakemore[a,]**

[a] Department of Chemistry, University of Kansas, 1567 Irving Hill Road, Lawrence, Kansas 66045, United States

[b] Oak Ridge National Laboratory, Chemical Sciences Division, Oak Ridge, Tennessee 37830, United States

* To whom correspondence should be addressed: blakemore@ku.edu (J.D.B.) and glezakouva@ornl.gov (V.-A.G.)

KEYWORDS: electrochemistry; reduction; oxo-activation; tris(pentafluorophenyl)borane; titrations

Abstract

Although it has been established that covalent functionalization of the U–O bonds in the uranyl dication (UO_2^{2+}) generally requires use of strong reductants and electrophiles, little work has examined how interactions between the individual reaction components could affect final outcomes in solution. Here, the patterns of such reactivity have been studied in a UO_2^{2+}-containing model system supported by a workhorse pentadentate ligand, 2,2′-[(methylimino)bis(2,1-ethanediylnitrilomethylidyne)]bis-phenol. Oxo activation and functionalization have been tested with *i)* electrochemical and chemical reduction, and *ii)* coordinating and non-coordinating solvents. In acetonitrile, uranyl reduction was achieved cleanly, but treatment of the reduced species with tris(pentafluorophenyl)borane (**BCF**) resulted in a mixture of products arising from direct electron transfer to **BCF**. In dichloromethane (CH_2Cl_2), electrochemical reduction of uranyl was achieved cleanly, but clean chemical reactivity was inaccessible. Despite these challenges, one trinuclear and oxo-deficient uranium-containing product was crystallized from CH_2Cl_2 solution and characterized; thus, desirable electrophilic reactivity can proceed to some degree in CH_2Cl_2 with **BCF**. Computational studies were used to investigate the properties of the trinuclear uranium product and the changes that could be inducible by further reduction. Taken together, the reactivity patterns identified here could inform design of improved systems for actinyl oxo functionalization.

Introduction

Significant progress has been made in recent years towards the reduction of the uranyl dication (UO_2^{2+}) in both aqueous and non-aqueous environments.[1,2] While uranyl in the +VI oxidation state (O.S.) is water soluble and mobile in aqueous environments, reduction to U(IV) results in solid

species that can be more easily isolated from the relevant media.[3,4] Reduction of U(VI) to U(IV), however, often involves generation of U(V) intermediates, and isolation of U(V) species has proven to be challenging due to the propensity of [UO_2^+] to undergo disproportionation reactivity under both oxic and anoxic conditions. Additionally, the *trans*-dioxo ligands on UO_2^{2+} precursors are quite stabilized by strong covalent bonds to U(VI), making uranyl with uranium in the +VI O.S. chemically inert to many reagents.[1] Indeed, uranyl is resistant to both reduction ($E°(U^{VI/V})$ = 0.16 V vs the standard hydrogen electrode; SHE)[5] and protonation in aqueous media, even by triflic acid.[6] U(V) species often engage in rapid self-disproportionation to yield U(IV) and U(VI) compounds, increasing the difficulties that can be encountered when attempting to gain control over and insight into the reactivity pathways that govern uranium redox chemistry and speciation.[7,8] Despite these challenges examples of complete oxo cleavage via chemical agents can be found,[7,9,10] including well-known photochemical routes.[11] Nonetheless, reports aimed at documenting the many possible reactivity pathways underlying uranyl reduction and functionalization have not appeared in the literature in great quantity,[12,13] although many reports exist that identify and present the products of such reactivity.

While the terminal oxo ligands in uranyl are only mildly basic when U is in the +VI oxidation state (O.S.), reduction to U(V) increases their basicity, motivating many oxo-functionalization strategies to involve association of an electrophile with the oxo(s) in tandem with reduction.[1] Dependent on the thermodynamic properties of the specific uranyl system of interest, one or more pathways to reduction and oxo-functionalization may be accessible. As shown in Scheme 1, a neutral uranyl(VI) complex could either engage directly with an electrophile (denoted as Z), or may require reduction before binding of the electrophile; alternatively, electrophile coupled electron transfer (ECET) could occur in a manner mimicking proton coupled electron transfer

(PCET).[14,15] Further reduction and functionalization can occur in certain cases to access bis-functionalized U(V) species or complexes of U(IV). In line with these idealized pathways, reports of direct coordination to the oxo(s) of uranyl(VI) by the strongly electrophilic tris(pentafluorophenyl)borane (**BCF**) are known, which result in a weakening of the U–O bond and allow for a more accessible U(VI/V) reduction (see the example product from Sarsfield and Helliwell in Scheme 2).[16,17] Some ligand systems preclude this possibility, however, necessitating reduction of uranyl(VI) to U(V) before electrophiles will engage in reactivity with the oxo moieties (see the work of Hayton and co-workers and one product shown in Scheme 2).[17,18,19] Many systems have been reported to follow the pathways involving discrete electron transfer and electrophile coordination,[1] but few systems are documented to engage in ECET; both the examples that appear to involve this pathway employ a silane reagent and yield a doubly oxo-functionalized product. This pathway would be associated formally with gain of $1e^-$ and two equivalents of electrophile Z in Scheme 1.[20,21,22,23,24,25] Finally, in a few systems, further controlled reduction to U(IV) is possible, giving rise to isolable bis-functionalized U(IV) species (see one example from Arnold, Love and co-workers in Scheme 2).[18,19]

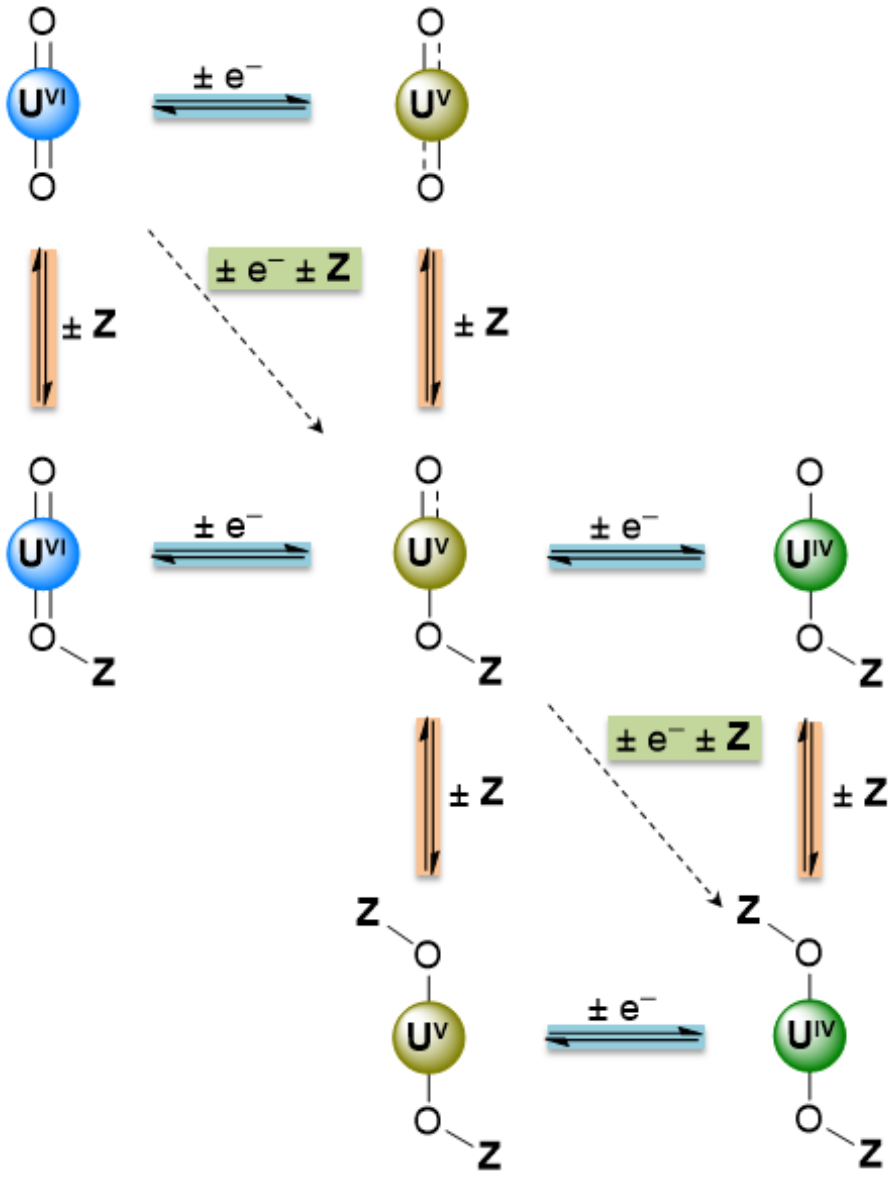

Scheme 1. Idealized pathways for electrophilic oxo-functionalization of a neutral uranyl(VI) compound (top left) promoted by reduction (Z = electrophile).

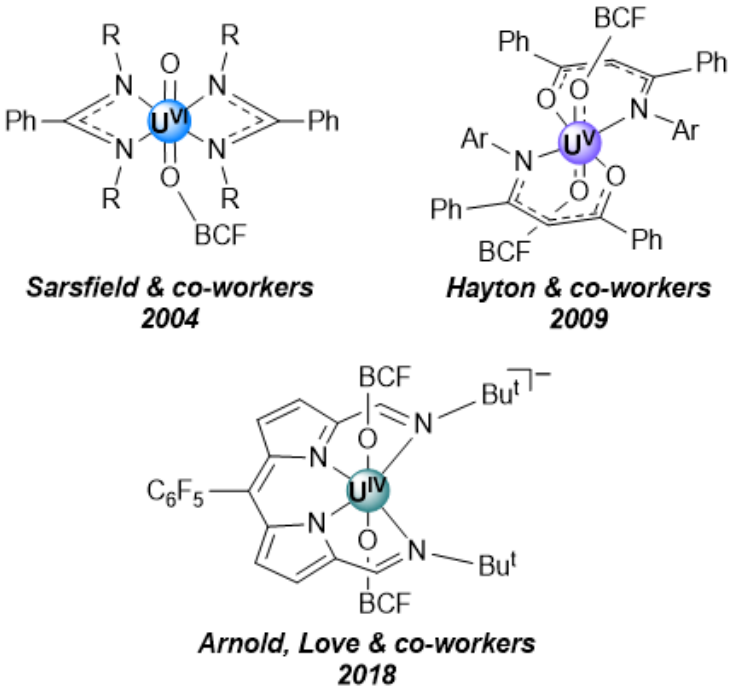

Scheme 2. Selected literature examples of BCF-functionalization products of uranyl in multiple oxidation states. BCF = tris(pentafluorophenyl)borane.

The outcome of reduction and oxo functionalization of uranyl varies widely depending on the equatorial coordination of U(VI), electrophile, reductant, and even solvent. Multidentate ligands are often chosen to support the uranyl core as they generally encourage the formation of molecular complexes whose reactivity can be more easily studied and allow for a greater degree of speciation control by limiting the available equatorial coordination sites. Monodentate atoms (e.g., halides) or small molecules (e.g., solvents) coordinated in this plane are typically labile and exchange of these can lead to formation of multiple species in solution.[26,27,28] In 2011, Ikeda and co-workers particularly highlighted the usefulness of a pentadentate ligand for avoiding these challenges,[29] building on earlier work from Mizuoka et al. showing that U(V) complexes supported by multidentate ligands are more stable than those supported by unidentate analogues as well as the

observation that multidentate ligands can disfavor disproportionation reactions of uranyl species.[30] In particular, a pentadentate ligand pioneered by Mazzanti and co-workers (denoted $\mathbf{L^{NM}}$ in this work) has been demonstrated to stabilize U(V) and does not contain any ionizable protons that could contribute to disproportionation reactivity under the reactive conditions of interest.[31] $\mathbf{L^{NM}}$ has the formal name 2,2′-[(methylimino)bis(2,1-ethanediylnitrilomethylidyne)]bis-phenol and was denoted ^{Me}saldien in some prior reports. $\mathbf{L^{NM}}$ and related ligands which are either tetradentate or feature an N–H group rather than an N–methyl group on the ligand have been studied by Takao and co-workers and have also been demonstrated to stabilize U(V) via spectroscopic methods.[32,33] These reports all build on the long-standing, established usefulness of salen-type ligands for binding the uranyl dication.[34] $\mathbf{L^{NM}}$ itself features an [N_3,O_2] cavity for the binding of uranyl, is easily prepared by a one-pot imine condensation reaction of salicylaldehyde and 2,2′-diamino-N-methyldiethylamine, and displays favorable electron-transfer properties in non-aqueous media, particularly acetonitrile-based electrolytes.[35] Of particular relevance to the current work, Takao and co-workers have reported both cyclic voltammetric studies and spectroelectrochemical work addressing formation of U(V) species from the U(VI) complex of $\mathbf{L^{NM}}$ in electrolyte solutions based on dimethylsulfoxide (DMSO) solvent.[33]

Aside from the many ligands that have been reported to form complexes of uranyl, a large variety of electrophiles have been employed in oxo-functionalization strategies, including alkali metal cations,[36,37,38] *p*-block elements,[39,40,41,42,43] transition metals,[12,20,44,45,46] and f-elements,[47,48] with **BCF** being one of the most common reagents.[7,10,16,17,18,19,22] Similarly, various chemical reductants have been employed, each with very negative potentials (as necessitated by the generally quite negative reduction potentials of the redox processes of uranyl complexes in non-aqueous media). As an alternative to chemical reductants, our group recently reported a unique

system in which a complex of uranyl(VI) could be reduced electrochemically and functionalized sequentially with a much milder electrophile, triphenylborane.[35] Considering the virtually endless options of reagents, solvents, and ligand systems that could be pursued in this arena, however, we anticipated that a systematic study in which both the desired *reactivity* of a uranyl(VI) complex with **BCF** and undesired *cross-reactivity* of the system would be useful for identifying patterns to inform future studies. We hypothesized that use of parallelized methodology with both coordinating and non-coordinating solvents and both electrochemical and chemical reduction would enable the identification, in particular, of specific combinations of reagents that cause deviations from the desired reactivity, and we thus refer to these suboptimal and undesired reactions as *cross-reactivity pathways* in this study. This study could aid in the design of future uranyl oxo-functionalization strategies from the perspective that the patterns identified here might inform selection of reagents aligned with the intrinsic Lewis acid/base chemistry and redox properties of uranyl.

Here, we report documentation of the reactivity and cross-reactivity that can be operational when a strong Lewis acid is used in the oxo-functionalization of uranyl across conditions involving coordinating and non-coordinating solvents and under electrochemically or chemically reducing environments. A reduced complex of the uranyl(V) monocation [UO_2^+] could be formed consistently in CH_3CN, but a mixture of products resulted when **BCF** was introduced due to disproportionation, decomposition, and other reactivity reported here. In the non-coordinating solvent CH_2Cl_2, the same uranyl(V) complex can be generated electrochemically, but efforts to prepare it with a chemical reductant (Cp^*_2Co) and induce reactivity with **BCF,** revealed cross-reactivity between Cp^*_2Co and **BCF**. It also resulted in decomposition of Cp^*_2Co in the CH_2Cl_2, as we recently reported in a preliminary communication.[49] The very Lewis acidic **BCF** electrophile

can, however, interact directly with the weakly Lewis basic oxo moieties of uranyl(VI) in CH_2Cl_2, as demonstrated by spectroscopic findings reported here. Reduction of the mixture containing U(VI) and **BCF** in CH_2Cl_2 gave rise, on one occasion, to a single crystalline product that was characterized by solid-state X-ray diffraction (XRD) analysis. Computational findings provide complementary insights into the experimentally observed differences in the electrophilicity of **BCF** in coordinating vs. non-coordinating solvents and provide evidence in support of the proposed oxidation states present in the structurally characterized product. On the basis of the systematic study presented here, we conclude that the multicomponent requirements of oxo functionalization can lead to intrinsic limitations in selectivity and efficiency. However, our findings also suggest opportunities for future improvements, particularly in matching of Lewis acidity/electrophilicity and uranium redox chemistry in order to avoid cross reactivity driven by unproductive electron transfer.

Results

Reduction of $U^{VI}O_2$. We have recently reported[35] the clean, highly reversible reduction reactivity of a model U(VI) complex, $\mathbf{U^{VI}O_2}$, to U(V) under both electrochemical and chemical conditions utilizing the solvent acetonitrile (structure of $\mathbf{U^{VI}O_2}$ shown in Scheme 3). Briefly, cyclic voltammetry data for $\mathbf{U^{VI}O_2}$ display a single accessible reduction at $E_{1/2}$ = –1.55 V vs ferrocenium/ferrocene (denoted hereafter as $Fc^{+/0}$) in electrolyte based on acetonitrile ($CH_3CN/TBAPF_6$; see SI, Figures S79 and S80) and at $E_{1/2}$ = –1.59 V (all potentials quoted vs. $Fc^{+/0}$) in electrolyte based on dichloromethane ($CH_2Cl_2/TBAPF_6$; see SI, Figures S85 and S86).[35,49,50] The identity of this reduction product in CH_3CN is a structurally similar complex $\mathbf{U^{V}O_2}$ that retains the intact uranyl moiety, albeit with the +V formal oxidation state. The pentadentate

equatorial coordination environment is also maintained in this species, which features an overall charge of –1.[35,50] Though some of the vibrational characteristics of $\mathbf{U^{V}O_2}$ have been previously reported by our group,[35] here we have added Raman spectra of $\mathbf{U^{VI}O_2}$ (15.4 mM) and $\mathbf{U^{V}O_2}$ (15.4 mM) in CH_3CN to our tabulation of the properties of this compound (Figure 1). The spectrum of $\mathbf{U^{VI}O_2}$ in CH_3CN displays a prominent ν_1 symmetric actinyl stretch at 799 cm^{-1}, which is in good agreement with the solid-state spectrum of this compound (ν_1 at 800 cm^{-1}).[51] Upon reduction of $\mathbf{U^{VI}O_2}$ by stoichiometric Cp^*_2Co to form the U(V) species $\mathbf{U^{V}O_2}$, this feature disappears and a new feature at 703 cm^{-1} (shifted from that in $\mathbf{U^{VI}O_2}$ by 96 cm^{-1}) can be seen which likely corresponds to the symmetric ν_1 stretch of the $[U^{V}O_2^{+}]$ unit. (Importantly, control spectra of $[Cp^*_2Co][PF_6]$ confirmed that the feature at 703 cm^{-1} corresponds to the uranyl-containing species $\mathbf{U^{V}O_2}$ rather than its counter-cation $Cp^*_2Co^{+}$). Few Raman spectra exist of U(V) compounds; one molecular U(V) example displays a shift in the ν_1 frequency of 75 cm^{-1} from its U(VI) counterpart[52] while uranyl dissolved in aqueous sodium carbonate displays a shift in the ν_1 frequency of 53 cm^{-1} upon conversion from the +VI to the +V O.S.[53] Thus, we suggest that the shift measured here of 96 cm^{-1} represents a reasonable change in the symmetric stretching frequency upon conversion of U(VI) to U(V).

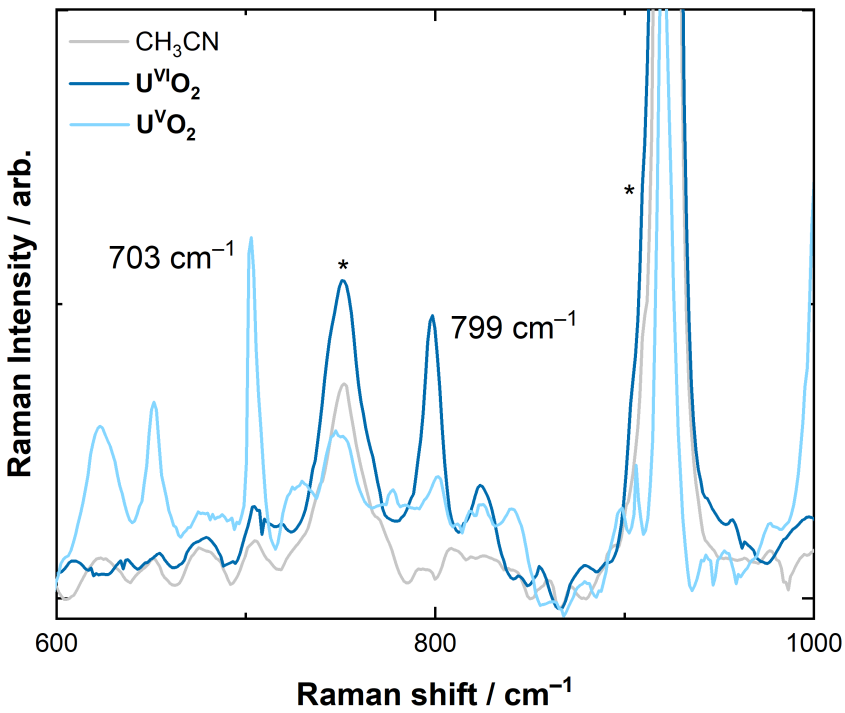

Figure 1. Solution-phase Raman spectra of CH_3CN (grey), $\mathbf{U^{VI}O_2}$ (15.4 mM in CH_3CN; dark blue), and $\mathbf{U^{V}O_2}$ (15.4 mM in CH_3CN; light blue). Features denoted with * correspond to stretches from the CH_3CN solvent.

A similar compound to $\mathbf{U^{V}O_2}$ (the same, formally speaking, to that generated in CH_3CN) is formed upon electrochemical reduction of $\mathbf{U^{VI}O_2}$ in CH_2Cl_2 as implicated by spectroelectrochemical data. To begin, the electronic absorption profiles of $\mathbf{U^{VI}O_2}$ are almost identical in CH_3CN and CH_2Cl_2, featuring ligand-based $\pi\rightarrow\pi^*$ transitions at 238 nm in CH_3CN or 248 nm in CH_2Cl_2 and LMCT transitions attributable to imine→U, phenoxide→U, and O_{yl}→U between 342–483 nm in CH_3CN or 348–482 nm in CH_2Cl_2 (see SI, Figures S65 and S70).[54,55] However, upon polarization of working electrodes immersed in solutions containing $\mathbf{U^{VI}O_2}$, reduction can be carried out in both acetonitrile- and dichloromethane-based electrolytes that results in formation of $\mathbf{U^{V}O_2}$. Spectroelectrochemistry with UV-visible detection was used to

reveal the spectral profile of $\mathbf{U^{V}O_2}$, based on comparisons to prior work from our group.[35,49] The profile obtained in CH_2Cl_2-based electrolyte resembles that of other similar U(V) complexes with strong ligand-based absorptions centered around 248 nm and a single additional absorption at 355 nm.[8,56]

Bulk electrolysis (BE) coupled to *ex situ* near-infrared spectroscopy was also used to interrogate the generation of $\mathbf{U^{V}O_2}$ in both acetonitrile- and dichloromethane-based electrolytes. In this experiment, pieces of highly oriented pyrolytic graphite were used as electrodes in a divided electrochemical cell to electrogenerate $\mathbf{U^{V}O_2}$ (in the working chamber) by reduction of $\mathbf{U^{VI}O_2}$. For this, ferrocene was used (in the auxiliary chamber) as a sacrificial reductant, providing the reducing equivalents needed for generation of U(V). (See Figure S76 for example photos of the electrochemical cell before, during, and after electrolysis.) Following extensive electrolysis at reducing potentials, samples of the working chamber solution were removed and interrogated by near-infrared (NIR) absorption spectroscopy. The resulting NIR spectra revealed the appearance of new weak transitions at 1385 nm in acetonitrile-based electrolyte and 1383 nm in dichloromethane-based electrolyte (see Figure 2, panels b and c). The features near 1400 nm are quite similar to each other and are consistent with 5*f*–5*f* transitions corresponding to an electrogenerated species with U(V) character. The measured features are attributable to the $5f^1$ electronic configuration, based on comparison to prior examples.[10,19,56,57,58] $\mathbf{U^{V}O_2}$ generated by BE is anionic in nature, and thus is paired with a tetrabutylammonium counter-cation (derived from the electrolyte). Appealingly, the NIR spectrum of $\mathbf{U^{V}O_2}$ generated by chemical reduction with Cp^*_2Co in prior work[35] (see Figure 2, panel a) compares well with those obtained here by BE. Notably, the molar absorptivity values for the *f*-to-*f* transitions obtained in the BE samples are similar to those obtained in the prior chemical work, providing strong support for the clean and

selective electrode-driven generation of U(V) in both the acetonitrile- and dichloromethane-based electrolytes. (See SI, pp. S43–S46 for details on the BE studies.)

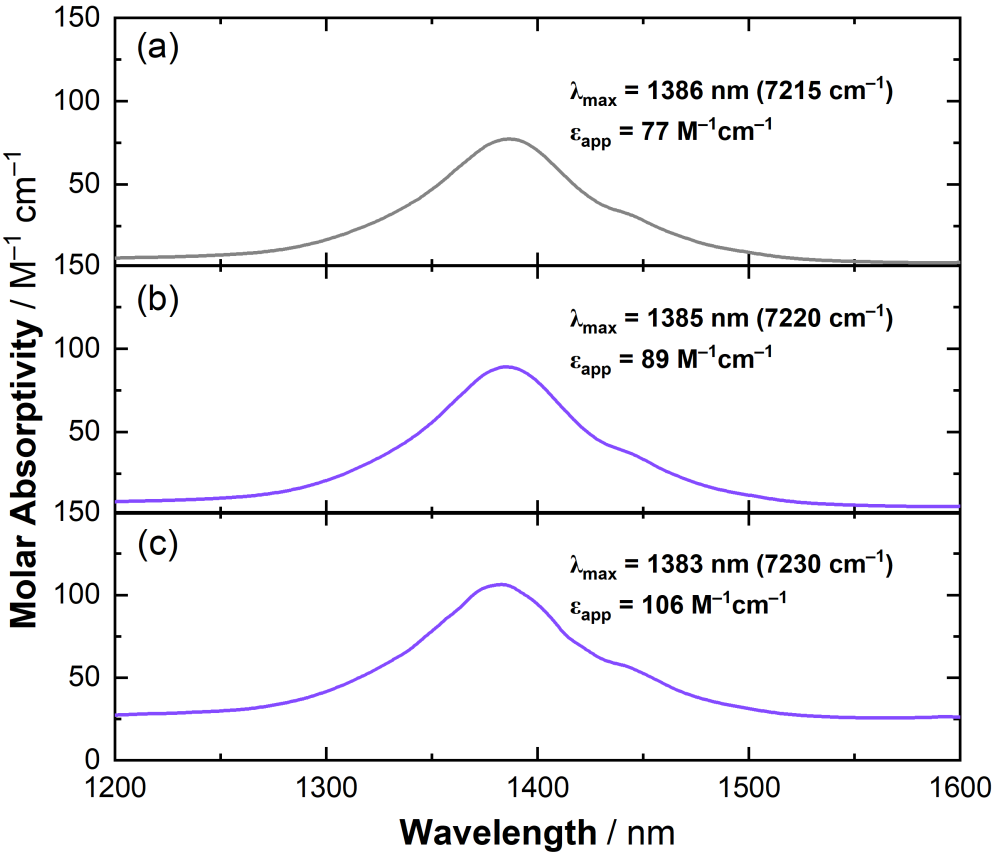

Figure 2. Near infrared spectra for $\mathbf{U^{V}O_2}$. Panel a: Data for $\mathbf{U^{V}O_2}$ generated by chemical reduction with stoichiometric Cp^*_2Co in CH_3CN. See reference 35 for details. Panel b: Data for $\mathbf{U^{V}O_2}$ prepared by bulk electrolysis (BE) in CH_3CN/$TBAPF_6$ (polarization at –1.62 vs $Fc^{+/0}$). Panel c: Data for $\mathbf{U^{V}O_2}$ prepared by BE in CH_2Cl_2/$TBAPF_6$ (polarization at –1.82 vs $Fc^{+/0}$ (middle). Apparent molar absorptivity values were calculated based on the measured spectral data and the anticipated concentration of the reduced uranium species based on chemical stoichiometry (panel a) as well as charge transferred in the BE runs (panels b and c).

In the reactivity involving a chemical reductant, though, the $\mathbf{U^{V}O_2}$ complex can also be cleanly isolated by the reduction of $\mathbf{U^{VI}O_2}$ by Cp^*_2Co in CH_3CN as reported in our prior work (see SI, Figure S67).[35,49] However, attempts to generate $\mathbf{U^{V}O_2}$ with Cp^*_2Co in CH_2Cl_2 ($E_{1/2}$ = –1.97 V in CH_2Cl_2/$TBAPF_6$) did not yield the anticipated clean reactivity when monitored by NMR and UV-visible spectroscopy (see SI, Figures S42 and S71). This alerted us to the possibility of undesirable side-reactivity in this non-coordinating solvent and led us to report the reactivity of Cp^*_2Co with CH_2Cl_2 in a prior communication.[49] Cp^*_2Co is unstable in CH_2Cl_2, and the reactivity underpinning this instability is summarized in Scheme 3. Unfortunately, this decomposition pathway implies that electron transfer reactions induced by Cp^*_2Co in CH_2Cl_2 are very unlikely to yield clean $1e^-$ reduction reactivity, an observation reflected in the consistent yields below 75% reported for reduction reactions carried out in related conditions.[17,59]

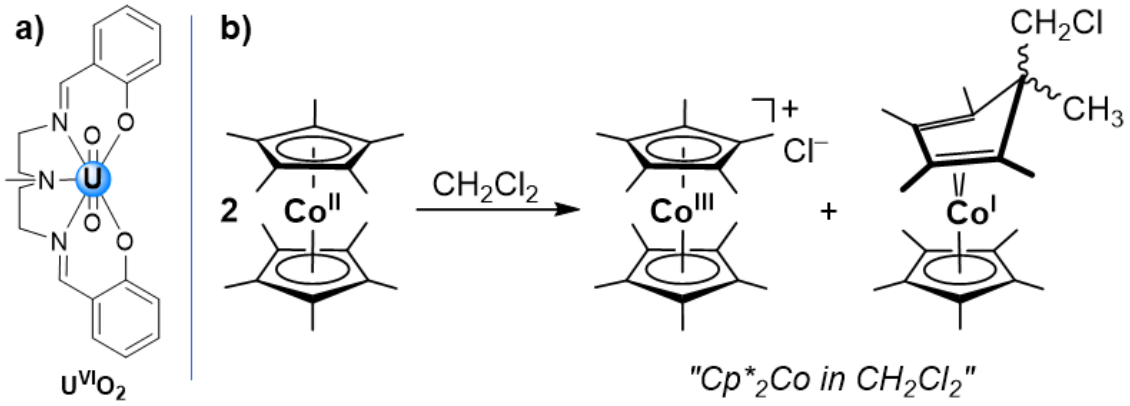

Scheme 3. a) Structure of $\mathbf{U^{VI}O_2}$. b) Reactivity of Cp^*_2Co with CH_2Cl_2.

Speciation of tris(pentafluorophenyl)borane in coordinating and non-coordinating solvents. Adduct formation of **BCF** with coordinating solvents is well-documented in several cases; X-ray diffraction data is available for the CH_3CN adduct of **BCF**, underscoring the innate

Lewis acidity of this reagent.[60,61,62,63] To provide context for our studies of uranyl reactivity with **BCF**, we monitored the formation of this adduct under our chosen conditions in both a coordinating and also a non-coordination solvent via infrared (IR) and NMR spectroscopies. On the one hand, we measured a shift in the C≡N stretching frequency of acetonitrile upon adduct formation with **BCF** from 2268 cm^{-1} to higher wavenumbers (2368 cm^{-1}; $\Delta\tilde{\nu}$ = 100 cm^{-1}), which is consistent with previously reported IR frequencies and contraction of the C≡N bond observed by XRD analysis (Δd_{C-N} = 0.033 Å; see SI, Figure S49).[63] On the other hand, the IR spectrum of **BCF** in CH_2Cl_2, shows excellent agreement with the attenuated total reflection (ATR) IR spectrum of **BCF** in the solid state, indicating that the effective electrophilicity of **BCF** in CH_2Cl_2 is similar to that of free **BCF** (see SI, Figures S47 and S51). The behavior of solid **BCF** and **BCF** dissolved in CH_2Cl_2 is anticipated to contrast starkly with the diminished effective electrophilicity in the coordinating solvent CH_3CN; this is indicated both by the change in the nitrile stretching frequency and the C–N bond length.

Effects of CH_3CN coordination on the properties of **BCF** are also apparent in ^{19}F NMR spectra, wherein the three distinct *ortho*-, *meta*-, and *para*-fluorine environments of the phenyl rings in **BCF** give rise to three signals that provide sensitive information about their respective electronic environments. For example, monitoring the ^{19}F NMR of **BCF** in CD_2Cl_2 as it was titrated with CH_3CN revealed a decrease in intensity of the **BCF** features at the expense of in-growth of three new, upfield resonances ($\Delta\delta$ = +5.24, +11.73, and +3.33 ppm, respectively; see SI, Figure S30). This suggests that the coordination of CH_3CN to **BCF** yields a strongly bound **BCF**–acetonitrile adduct (denoted as **BA**), effectively increasing the electron density and steric crowding about the boron center in **BCF** and generally decreasing its electrophilic nature. Furthermore, a sharp signal, which is indicative of a tetrahedral boron center, is present in the ^{11}B

NMR of **BCF** in CD_3CN at –12.2 ppm (see SI, Figure S3; literature reported shift for **BA**: ^{11}B NMR (C_6D_6) δ = –10.3 ppm).[63] This signal contrasts with that corresponding to **BCF** in the ^{11}B NMR taken in CD_2Cl_2, which appears as a broad feature at +52.6 ppm (see SI, Figure S25; literature reported shift for **BCF**: ^{11}B NMR (CD_2Cl_2) δ = 59.8 ppm).[64] Together, this evidence supports the formation of **BA** under our chosen conditions in CH_3CN and demonstrates that the electronic and structural properties of the solvated **BCF** electrophile vary widely depending on the coordinating or non-coordinating nature of its solvent environment.

Cross-reactivity between electrophile, electrolyte, and reductant. Informed by literature reports regarding the reactivity of **BCF** with polyatomic anions, the incompatibility of **BCF** with $TBAPF_6$ in CH_2Cl_2 could be anticipated in an electrochemical/electrolyte context. Indeed, we observed this under our conditions. NMR spectra of a **BCF**/$TBAPF_6$ mixture in CD_2Cl_2 show peaks associated with a **BCF**-containing species that are shifted drastically upfield and the absence of ^{31}P resonance associated with $TBAPF_6$ (see SI, Figure S33 and S34). In the ^{31}P spectrum of this mixture, a quartet at δ = –34.9 ppm (J_{PF} = 1072 Hz) can be seen corresponding to phosphoryl fluoride (OPF_3), a species which also gives rise to a doublet in the ^{19}F spectrum of this mixture at δ = –88.5 ppm (J_{PF} = 1072 Hz; literature reported shifts for OPF_3: ^{31}P NMR ($CDCl_3$) δ = –33.9 ppm, J_{PF} = 1072 Hz and ^{19}F NMR ($CDCl_3$) δ = –88.6 ppm, J_{PF} = 1073 Hz).[65,66] Phosphoryl fluoride can form from the partial hydrolysis of PF_5 which was likely generated under our conditions by **BCF**-induced halide abstraction from PF_6^- and subsequent reaction with adventitious water present in the NMR solvent (halide abstraction from PF_6^- by **BCF** has been previously reported).[65,67] Consistent with this reaction sequence and the identity of the **BCF**-containing product, a set of resonances associated with $[(BCF)F]^-$ were observed from the same sample by ^{19}F NMR spectrum at δ = –134.2, –158.0, –165.9, and –190.0 ppm (literature shifts of $[^nBu_4N][B(C_6F_5)_3F]$: ^{19}F NMR

($CDCl_3$) δ = –133.9, –159.9, –164.6, and –185.2 ppm; literature shifts of $[Ph_3C][B(C_6F_5)_3F]$: ^{19}F NMR (C_7D_8) δ = –134.8, –161.9, –166.2, and –187.0 ppm).[67,68] A distinctive signal that could correspond to $[(BCF)F]^-$ can also be seen in the ^{11}B NMR of the mixture of **BCF** and $TBAPF_6$ in CD_2Cl_2 at –0.51 ppm (see SI, Figure S35; literature reported shift for $Cs^+[(BCF)F]^-$ ^{11}B (d_6-DMSO) δ = –0.86 ppm).[69] In any case, the upfield shifts of the $[(BCF)F]^-$ resonances in both the ^{19}F and ^{11}B spectra compared to those of **BCF** are characteristic of both increases in the boron-centered electron density and an increase in the coordination number of the boron center. All of these features notwithstanding, **BCF** appears stable in dichloromethane that is free of $TBAPF_6$. This latter conclusion was based on the quite satisfactory agreement between the values associated with the ^{19}F NMR resonances observed in the course of our work and those previously reported for this compound in CD_2Cl_2.[70]

With regards to its electrochemical properties, reductive characterization of **BCF** has been hindered in the past by reactivity with the anions of common supporting electrolytes (i.e., ClO_4^-, PF_6^-, and BF_4^-), with most previous attempts yielding ill-defined waves. The quasi-reversible reduction of **BCF** was measured, however, in 2011; the data from this study revealed a quasi-reversible couple ca. $E_{1/2}$ = –1.6 V vs $Fc^{+/0}$ in both non-coordinating solvent (CH_2Cl_2) and weakly interacting $[^nBu_4N][B(3,5\text{-}(CF_3)_2C_6H_3)_4]$ (i.e., [TBA][$BArF_{24}$]) as the supporting electrolyte. In the data, the re-oxidation of $[B(C_6F_5)_3]^{\cdot-}$ could only be observed at high scan rates, suggesting the radical undergoes significant reactivity after formation at the electrode, a finding also consistent with our work here.[71] We anticipated that the observation of reactivity of **BCF** with most electrolytes could be modulated, however, by the Lewis basicity of the solvent used for the electrochemical investigations; a more basic solvent might play a role in "protecting" **BCF** from

decomposition in the presence of species (like PF_6^-) with which it may irreversibly react to form adducts, such as $[(BCF)F]^-$.

Along this line, we hypothesized that formation of an alternative adduct via a pathway with a lower activation energy with coordinating solvent could kinetically preclude a reaction with a higher barrier, such as fluoride abstraction from PF_6^-. On the one hand, the coordinating solvent environment afforded by use of tetrahydrofuran (THF) does not appear to be sufficient to protect **BCF** from reactivity on the basis of literature studies.[72] On the other hand, in line with our theory, we have found that there is virtually no reactivity between **BA** and PF_6^- in the coordinating system of $CH_3CN/TBAPF_6$. Support for this finding was obtained through ^{19}F and ^{31}P NMR wherein no evidence for degradation of **BA** or $TBAPF_6$ could be measured when mixtures were combined in 1:1 or 1:5 ratios in CD_3CN (see SI, Figures S10–S13). These data indicate that coordination of CH_3CN to **BCF**, resulting in formation of the adduct $(C_6F_5)_3B–NCCH_3$ (**BA**) imparts sufficient stability to protect the boron center from reactivity with PF_6^-. To capitalize on this finding, we next probed the cyclic voltammetry of **BA** in $CH_3CN/TBAPF_6$. The resulting voltammograms revealed an irreversible reduction event at –2.46 V and no corresponding re-oxidation in the scan rate-dependent data up to 300 mV/s (see SI, Figures S77 and S78). Across all scans, however, the current response remained measurable as a result of the increased stability of **BA** compared to **BCF** in a non-coordinating environment (see SI, Figure S84). Taken together, these findings imply that significant follow-up chemical reactivity occurs upon formation of the $[B(C_6F_5)_3]^{\cdot-}$ radical anion. This agrees well with the prior reactivity of the radical that was documented in CH_2Cl_2.[71,73] Compared to the reported cathodic peak potential in the $CH_2Cl_2/[^nBu_4N][B(3,5\text{-}(CF_3)_2C_6H_3)_4]$ system, the reductive feature in $CH_3CN/TBAPF_6$ is shifted to significantly more negative potentials ($\Delta E_{p,c}$ = ca. 860 mV). This shift to a more negative reduction potential may be attributed

to the increase in electron density resident on **BA** arising from the bound CH_3CN in comparison to the bare **BCF** present in the CH_2Cl_2 electrolyte.

Turning to the question of direct chemical reduction of **BCF** by a chemical redox reagent, we mixed **BCF** and Cp^*_2Co in CD_2Cl_2 and collected ^{19}F and ^{11}B NMR spectra for this mixture. We observed a single fluorine-containing product in the data, corresponding to formation of $[(BCF)Cl]^-$, with an accompanying ^{11}B feature at –7.2 ppm (see SI, Figures S31 and S32; literature shifts of $[(BCF)Cl]^-$: ^{19}F NMR (CD_2Cl_2) δ = –132.5, –162.1, and –166.9 ppm, ^{11}B NMR (CD_2Cl_2) δ = –7.0 ppm).[74] Two additional sharp features are present in the ^{11}B NMR spectrum of this mixture at –0.9 and –3.8 ppm which could correspond to other tetrahedral boron side products (literature shift of $[B(C_6F_5)_2H]^-$: ^{11}B (CD_2Cl_2) δ = –0.9 ppm and $[B(C_6F_5)_2Cl]^-$: ^{11}B (CD_2Cl_2) δ = –3.8 ppm).[73] These observations are consistent with our prior work on reactivity between dichloromethane and Cp^*_2Co; as mixing these two reagents results in significant radical reactivity and the generation of chloride (see Scheme 3), the vast excess of dichloromethane in this experiment appears to promote solvent reactivity with the reducing agent, followed by chloride capture by **BCF**.

On the one hand, this proposed reaction sequence is in accord with the measured reduction potential of Cp^*_2Co, which is more than 300 mV negative of the reduction potential for **BCF** in CH_2Cl_2 ($E_{1/2}$ of $[Cp^*_2Co]^+/Cp^*_2Co$ = –1.97 V vs $Fc^{+/0}$ in CH_2Cl_2 electrolyte). On the other hand, at first glance, reduction of **BA** by Cp^*_2Co would not be expected to occur to a significant degree in CH_3CN as the reduction potential of Cp^*_2Co in CH_3CN media is more than 500 mV positive of the reduction potential for **BA** in $CH_3CN/TBAPF_6$ measured here ($E_{1/2}$ of $[Cp^*_2Co]^+/Cp^*_2Co$ = –1.91 V vs $Fc^{+/0}$ in CH_3CN electrolyte).[49,71,75] (See Figures S77 and S78 for voltammetry data for **BA**). Nevertheless, evidence for chemically driven reduction of **BA** by Cp^*_2Co in CH_3CN media

was obtained with multiple experiments/techniques. The ^{1}H NMR spectrum resulting from the mixture of **BA** with Cp*$_2$Co shows a set of broad, shifted resonances between 8 and 14 ppm, rather than the characteristic broad resonance near 47 ppm for Cp*$_2$Co or the intense singlet of [Cp*$_2$Co]$^+$ near 1.7 ppm that would be expected if electron transfer took place (see SI, Figures S8). With respect to the fluoride-containing species, two products can be detected from the mixture of **BA** with Cp*$_2$Co in CH_3CN via ^{19}F NMR and Mass Spectrometry in negative ion mode. The mass spectrum of this mixture diluted with methanol reveals two primary species with *m/z* (M^+) = 528.9901 and 543.0039 corresponding to the $[B(C_6F_5)_3OH]^-$ and $[B(C_6F_5)_3OCH_3]^-$ anions, respectively (see SI, Figures S62–S64).[76] These two species correspond to six total resonances in the ^{19}F NMR spectrum between –135 and –169 ppm, which are in good agreement with the literature reported values for these compounds (see SI, Figure S9).[77,78] The formation of these species is likely derived from reactivity of *in situ* generated $[B(C_6F_5)_3]^{\cdot-}$ with adventitious water (and/or added methanol) in the absence of other oxygen sources. Finally, a time-based reactivity study of Cp*$_2$Co with **BA** monitored by UV-visible spectroscopy reveals that BA can be reduced by Cp*$_2$Co in CH_3CN on the order of minutes, with absorbance of the in-situ generated [Cp*$_2$Co]$^+$ levelling off after approximately 200 seconds after mixing (Figure 3). Considering the coherent body of evidence from these reactivity and cross-reactivity studies, the use of very strongly Lewis acidic electrophiles appears to place an inadvertent limitation on clean reductive oxo-activation strategies that can be explored for uranyl (reactivity summarized in Scheme 4). Combining potent reagents induces prolific, undesirable cross-reactivity that could be avoided, as evident when compared to the beautifully clean electrochemical and chemical activation of the uranyl ion that can be achieved when a milder Lewis acid, triphenylborane, is employed.[35]

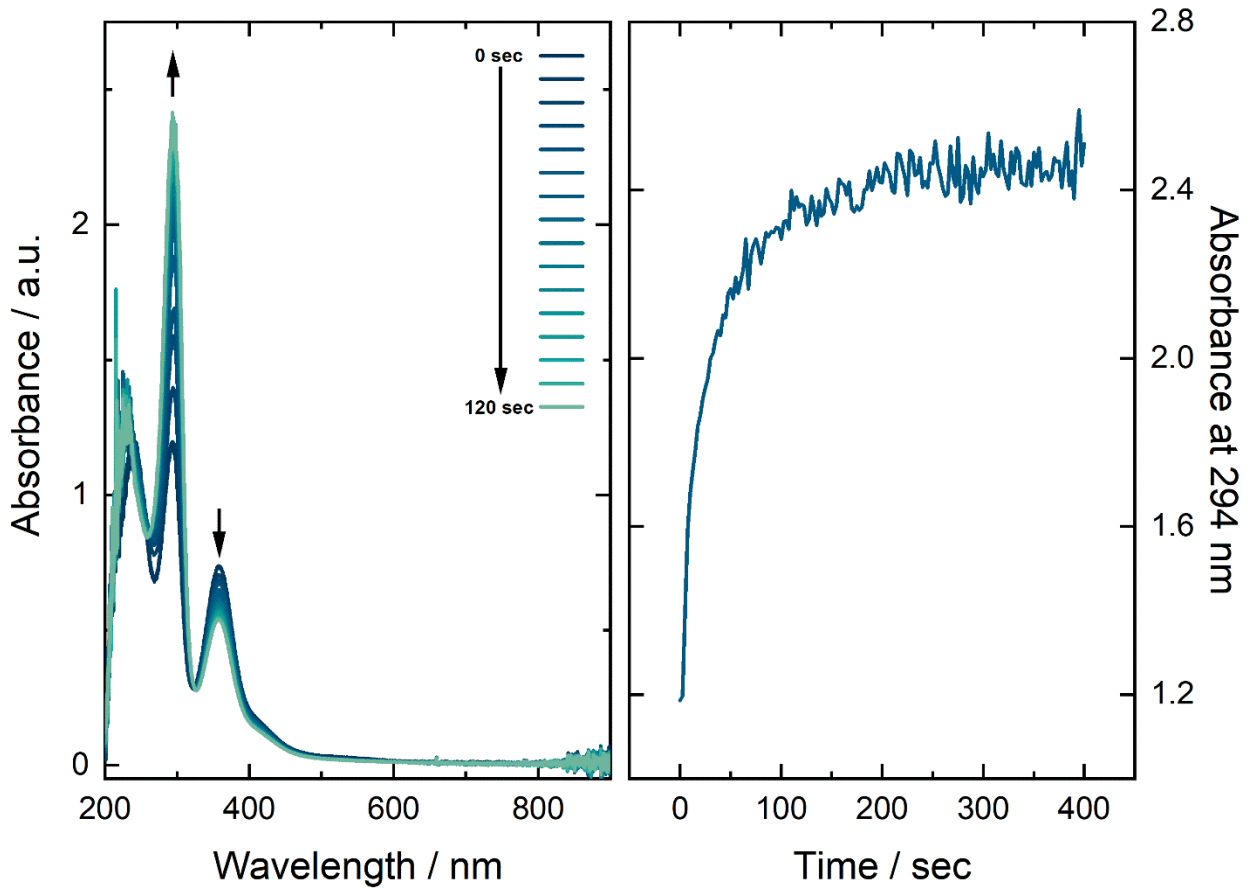

Figure 3. Spectral changes resulting from the addition of **BA** to Cp^*_2Co in CH_3CN as monitored by UV-Visible spectroscopy.

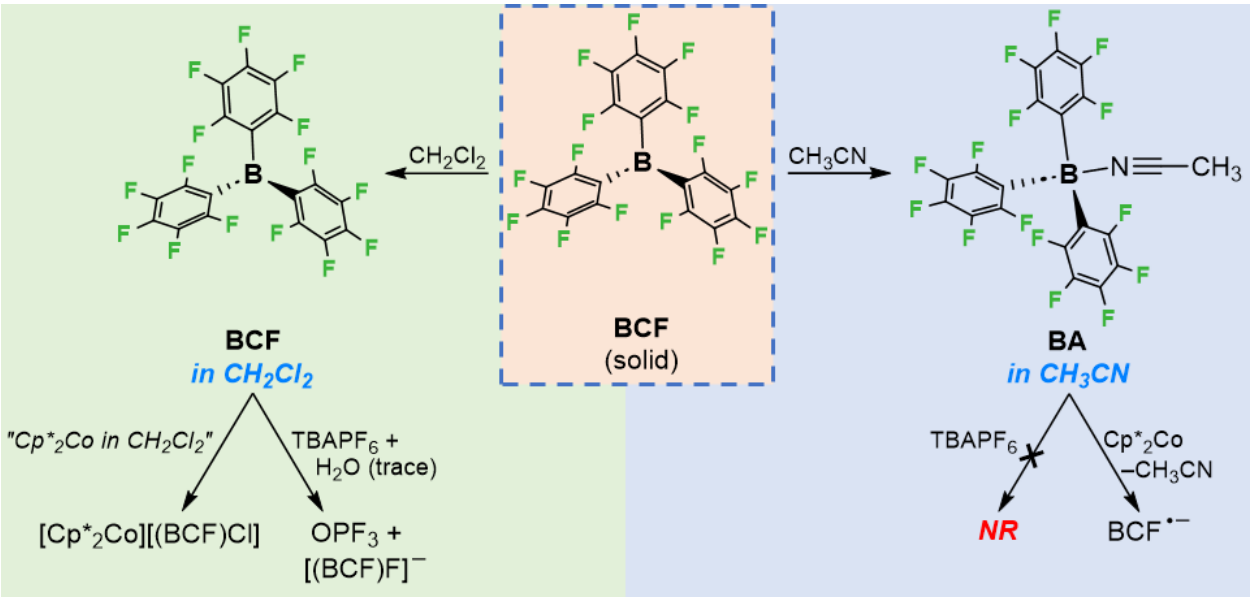

Scheme 4. Summary of all species directly detected from the cross-reactivity between BCF and commonly used reagents including solvents, a chemical reductant (Cp^*_2Co) and an electrolyte ($TBAPF_6$).

Reactivity of $U^{VI}O_2$ with BCF in coordinating and non-coordinating solvents. Consistent with the diminished Lewis acidity of the solvent adduct **BA** in comparison to **BCF**, no reaction was observed between $\mathbf{U^{VI}O_2}$ and **BA** via NMR or UV-visible spectroscopies. On the NMR side, this was evident by the absence of any shifted or new peaks in the ^1H and ^{19}F NMR spectra of these reaction mixtures. In the optical work, there was little change in absorption maxima when the reagents were mixed (see SI, Figures S14–S17).

However, in line with the greater Lewis acidity of **BCF**, significant reactivity ensues between $\mathbf{U^{VI}O_2}$ and **BCF** in CH_2Cl_2, conditions under which the **BCF** molecule is not bound by solvent or any other Lewis base prior to exposure to $\mathbf{U^{VI}O_2}$. Multiple diamagnetic species were observed in ^1H NMR spectra of the reaction of $\mathbf{U^{VI}O_2}$ with 1 and 2 equivalents of **BCF**, including $\mathbf{U^{VI}O_2}$ as well as two other major species that are shifted compared to the peaks of $\mathbf{U^{VI}O_2}$ (see SI, Figures

S36 and S38). The splitting patterns and number of peaks observed for the two new species could be consistent with the retention of the C_s symmetry of $\mathbf{U^{VI}O_2}$ in solution, suggesting that interaction with **BCF** could be occurring through coordination of the terminal oxo ligands of the uranyl unit to the acidic boron center and could give rise to a mixture of borylated species in solution that may be in equilibrium with each other (see Figure S41). However, mixing $\mathbf{U^{VI}O_2}$ and either 1 or 2 equiv. of **BCF** clearly resulted in reactivity that is neither clean nor selective, based on additional minor resonances that were observed by ^{1}H NMR (see Figure S41). Interaction of **BCF** with the phenoxide donors bound to uranium does not appear to be a major contributor to the observed spectral changes, since it is likely that engagement in this coordination mode would result in significant desymmetrization of the compound and signals resembling those of the non-complexed, uranium-free organic backbone of $\mathbf{L^{NM}}$; however, there is evidence from ^{1}H NMR and infrared spectroscopy for some generation of one or more products that have undergone loss of UO_2^{2+} from chelated $\mathbf{L^{NM}}$, resulting in spectral signals attributable to H-bonded phenol species (see SI, p. S25 and Figures S41, S52, S54, and S56). Regarding the apparent major products, however, there is an overall downfield shift observed in the ^{1}H NMR spectrum for numerous resonances. Taken along with the general upfield shift of the resonances of **BCF** measured in ^{19}F NMR spectroscopy upon mixing with $\mathbf{U^{VI}O_2}$ (see SI, Figure S37 and S39), these findings support the possibility of oxo-binding of one or more **BCF** molecules. This is because, in such binding, the uranyl unit would become more electron deficient and the **BCF** moiety would become more electron rich. Evidence for such interactions is also apparent in the ^{11}B NMR spectrum of the reaction of $\mathbf{U^{VI}O_2}$ with 2 eq. **BCF** in CD_2Cl_2 which shows sharp features (–3.6 and –10.8 ppm; see SI, Figure S40) that are significantly shifted compared to free **BCF** in CD_2Cl_2 (+52.6 ppm). Such sharp and upfield signals are conventionally associated with species displaying tetrahedral

geometry at boron, as would be expected if **BCF** were to interact directly with the oxo groups of the uranyl dication.

Vibrational spectroscopy provides further support for the formation of the proposed **[$U^{VI}O_2$(BCF)$_2$]** intermediate as a major reaction product of mixing **$U^{VI}O_2$** and 2 eq. of **BCF** (see SI, Figures S52–S57). Both the solid-state and solution IR spectra were obtained to investigate formation of **[$U^{VI}O_2$(BCF)$_2$]**. For this effort, **$U^{VI}O_2$** with 2 eq. **BCF** were reacted in CH_2Cl_2 then the solvent was removed *in vacuo*. This dried sample was then used to obtain the solid-state IR spectrum, or it was immediately redissolved to obtain the solution spectrum. In both cases, there is a drastic decrease in the intensity of the υ_3 asymmetric uranyl stretch (which appears at 883 cm^{-1} in free **$U^{VI}O_2$**); this is indicative of conversion of the majority of starting **$U^{VI}O_2$** to another species. Additionally, there remains a minor feature near the frequency of the υ_3 feature of **$U^{VI}O_2$**, albeit shifted slightly by 4 cm^{-1} to lower wavenumbers; this feature could be indicative of an equilibrium of **BCF** association with uranyl. We note however that this shift is not as pronounced as that (23 cm^{-1}) which was previously observed for a similar borylated species via Raman spectroscopy.[16] Other shifted features corresponding to both the **BCF** moiety and the organic ligand backbone surrounding uranyl can also be seen in the fingerprint region, though the imine stretch (for U-bound **L^{NM}**) in the presumed **[$U^{VI}O_2$(BCF)$_2$]** intermediate is present at 1611 cm^{-1}, similar with respect to the **$U^{VI}O_2$** precursor. This suggests that uranyl is not removed, in large measure, from the ligand by **BCF,** as the imine stretch of the free ligand appears at 1629 cm^{-1} and would be visible in these spectra if a significant pool of free **L^{NM}** ligand were present.

Solution- and solid-state Raman spectra were also collected to interrogate the proposed **[$U^{VI}O_2$(BCF)$_2$]** intermediate. Unfortunately, the spectra of the solid samples for Raman that were prepared in an analogous fashion to the solid-state IR samples revealed only features

corresponding to $\mathbf{U^{VI}O_2}$ and **BCF** which do not appear to be interacting with each other (see SI, Figure S58–S60). We note, however, that the solid-state Raman spectra in this study were collected multiple days after preparation (due to instrument availability and sample-preparation logistics) and thus we propose that the $\mathbf{[U^{VI}O_2(BCF)_2]}$ species may not be stable at room temperature on this time scale (days), hence the noted decomposition and the observation of primarily the $\mathbf{U^{VI}O_2}$ starting material. However, the solution-state Raman spectra of the reaction of $\mathbf{U^{VI}O_2}$ (20 mM) with 2 eq. **BCF** in CH_2Cl_2 (taken on the same day, within hours, of sample preparation) show a feature at ca. 760 cm^{-1} which is a shoulder to a solvent-derived stretch and could be attributable to the presence of the possible $\mathbf{[U^{VI}O_2(BCF)_2]}$ intermediate that is supported by the other spectroscopic studies reported here (see SI, Figure S61). This feature, when compared to the υ_1 symmetric stretch of the uranyl core of starting $\mathbf{U^{VI}O_2}$, shifts to lower energy by ca. 40 cm^{-1}. This is reasonable considering the 23 cm^{-1} shift observed for the association of a single **BCF** moiety with a uranyl(VI) complex that was documented by Sarsfield and Helliwell.[16]

In accord with all these findings from NMR and vibrational spectroscopies, monitoring the reaction of $\mathbf{U^{VI}O_2}$ with **BCF** in CH_2Cl_2 by UV-visible spectroscopy shows the evolution of the spectral profile of $\mathbf{U^{VI}O_2}$ into new species (based on the other spectroscopic work described above, multiple new species) with absorption maxima at 289 and 387 nm (see Figure 4). The UV-visible data collected on the reaction appear to show production of more than one product, however, as isosbestic behavior was not observed. This finding is again consistent with the detection of multiple species by NMR and the hypothesis that equilibria could be involved in the interactions between **BCF** and the uranyl core of $\mathbf{U^{VI}O_2}$ in the solution phase. Perhaps in accord with the synthesis and characterization of very few uranyl complexes supported by organic ligand frameworks featuring **BCF** bound to the terminal oxo atoms in the U(VI) formal oxidation state,[16]

further attempts at clean isolation of complexes of uranyl(VI) with **BCF** in this system were unsuccessful. Nonetheless, taken together, the available spectroscopic data suggest that a metastable product of mixing 2 equivalents of **BCF** and $\mathbf{U^{VI}O_2}$ is $\mathbf{[U^{VI}O_2(BCF)_2]}$, a species that complements the BCF-bound uranyl(VI) complex that was isolated and fully characterized by Sarsfield and Helliwell.[16]

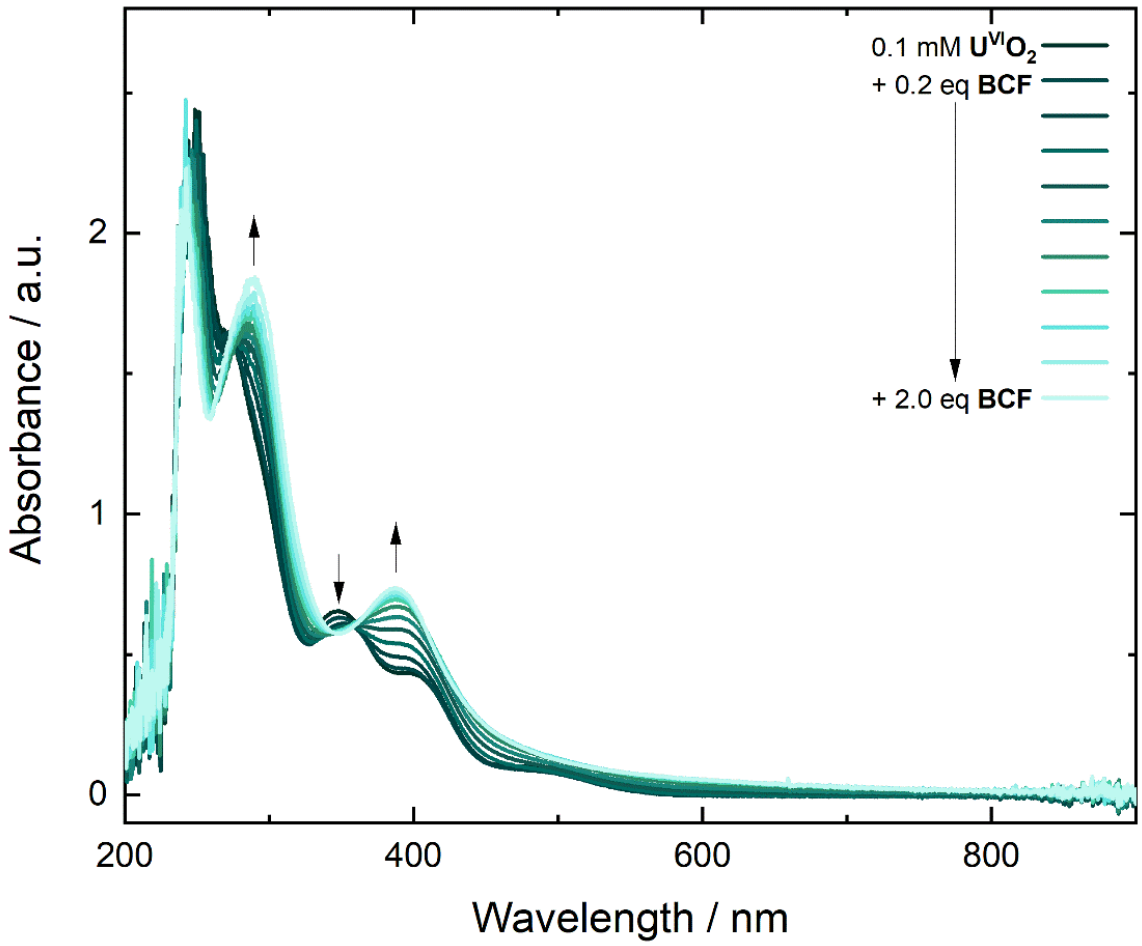

Figure 4. Spectral changes resulting from the addition of **BCF** to $\mathbf{U^{VI}O_2}$ in $\mathbf{CH_2Cl_2}$ as monitored by UV-Visible spectroscopy.

Reactivity of $U^{V}O_2$ with BA in CH_3CN. With the clean generation of **$U^{V}O_2$** in CH_3CN under chemical/electrochemical conditions established on the basis of the spectroscopic results, as well as the baseline reactivity established for each of the individual components, we next investigated the electrochemical activation of **$U^{VI}O_2$** with **BCF** by pursuing reduction of U(VI) to U(V) in the presence of **BCF**. Beginning with **$U^{VI}O_2$** in $CH_3CN/TBAPF_6$, incremental additions of **BA** in $CH_3CN/TBAPF_6$ were made to the electrochemical cell. There were significant changes to the cyclic voltammetry profile, suggesting that reactivity does occur in this system (see Figure 5). Beginning at ca. –0.5 V and scanning cathodically, cathodic current flow near –1.25 V was found to increase as increasing amounts of **BA** were added to the electrochemical cell. While current flow of this sort, positive of the main U^{VI}/U^{V} reduction wave, could be associated with a pre-equilibrium association step between **$U^{VI}O_2$** and **BCF**, we anticipate that such an equilibrium is negligible in this system between **$U^{VI}O_2$** and **BA** based on the spectroscopic evidence presented above. The more likely scenario for the increasing cathodic current at these potentials is a rapid reaction of the nascent U(V) form of the uranyl complex with the added **BA**. Support for this assignment comes from consideration of the classical characteristics of reactivity that is sufficiently fast to promote so-called kinetic potential shifts.[79] In such a case, reaction of **BA** with **$U^{V}O_2$** would be fast on the electrochemical timescale, resulting in perturbation of the Nernstian equilibrium associated with electron transfer to/from the unfunctionalized uranyl complex, resulting in turn to an apparent positive shift of that redox manifold in the presence of **BA**. As would be anticipated for such a case, the current flow at –1.25 V increases as a function of [**BA**] (see SI, Figure S81).[80,81] In the reaction of the U(V) complex with **BCF**, we anticipate that the CH_3CN equivalent bound to **BCF** as in **BA** would be displaced by the more Lewis basic terminal oxo ligands of the $[UO_2^{+}]$ unit. On the anodic branch (return sweep of the CV), the oxidation of

the electrogenerated $\mathbf{U^{V}O_2}$ becomes progressively less reversible as the availability of **BCF**/**BA** is increased. This is consistent with follow-up reactivity between $\mathbf{U^{V}O_2}$ and the added borane, as the electrogenerated $\mathbf{U^{V}O_2}$ is depleted from the reaction-diffusion layer near the electrode surface when **BA** is present. Indeed, the return oxidation wave is completely absent when 1 equiv. of **BA** is present in the solution.

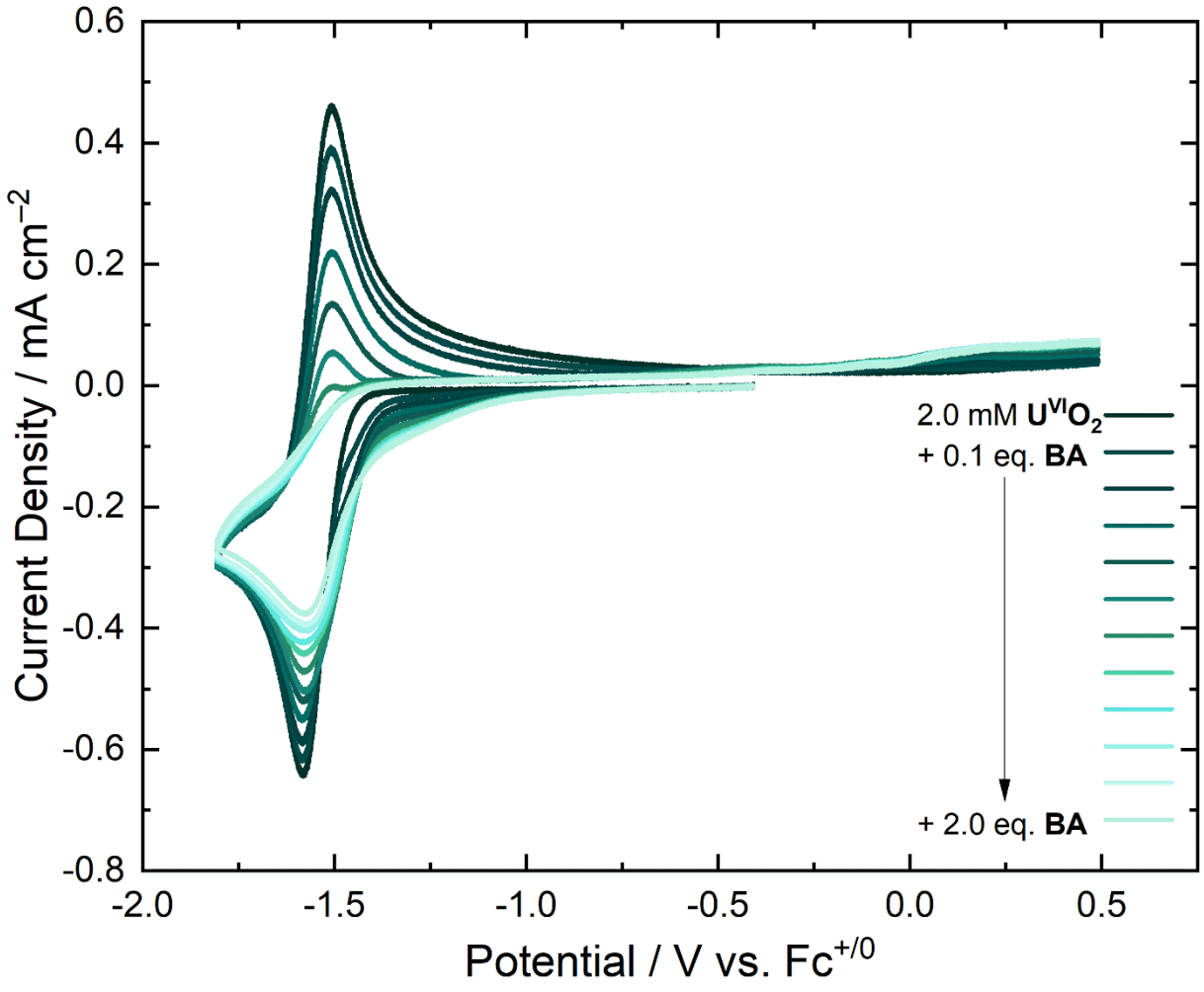

Figure 5. Electrochemical titration of $\mathbf{U^{VI}O_2}$ with **BA** in CH_3CN/$TBAPF_6$ (scan rate: 100 mV/s, first scans shown).

As evident in the voltammetry data shown in Figure 5, there are no significant or well-defined oxidation waves that appear in the data at potentials positive of the couple associated with $\mathbf{U^{VI}O_2}$/ $\mathbf{U^{V}O_2}$ redox cycling, even after multiple scans (see SI, Figure S83). This suggests that the reaction product(s) that result from reaction of $\mathbf{U^{V}O_2}$ with **BA** may not have readily accessible oxidation processes under these conditions, may be associated with slow heterogeneous electron transfer kinetics, or may not be soluble/available at the electron surface for re-oxidation upon generation. However, we did observe broad waves with modest oxidizing currents at rather positive potentials (E_{onset} of ca. –0.2 V and extending to 0.5 V) in the data (see SI, Figure S82). We anticipate that these currents are associated with re-oxidation of reduced products formed at the electrode. As these currents appear in the data only when scanning to potentials associated with reduction of $\mathbf{U^{VI}O_2}$ and in the presence of **BA**, we anticipate the species undergoing reoxidation likely arise from reactivity involving uranium. In accord with this proposal, the oxidizing currents associated with the processes between –0.2 and 0.5 V persisted in all relevant cycles of voltammetry interrogated in this system, and increased upon addition of up to 2 equiv. of **BCF** with respect to the initial $\mathbf{U^{VI}O_2}$ concentration. Like all the other data presented, these observations support interaction of **BA** with $\mathbf{U^{V}O_2}$ upon generation. Notably, it is unlikely that redox (electron transfer) reactivity occurs between **BA** and $\mathbf{U^{V}O_2}$, as $\mathbf{U^{V}O_2}$ is not likely to be able to reduce **BA** on the basis of the very negative reduction potential of **BA** in CH_3CN/$TBAPF_6$ ($\Delta E_{\boldsymbol{U^{V}O_2-BA}}$ = –0.91 V).

Considering all of the findings from the electrochemical work, we anticipate that reduced and borylated species are produced under the electrochemical conditions by rapid reaction of $\mathbf{U^{V}O_2}$ with **BA**. This finding is similar to that in our group's related work with triphenyl(borane) as electrophile in an electrochemical reactivity scheme, although in the latter case the borylated species showed more well-behaved electrochemical properties upon formation.[35] We thus wish to

emphasize here that substitution of **BCF** for triphenylborane appears to drive increased reactivity, but also induces irreversible behaviors that cloud identification of molecular reactivity pathways in the voltammetry data beyond the initial uranium reduction.

Spectrochemical titrations of $\mathbf{U^{V}O_2}$ with **BA** were carried out to better understand the reaction products that result from this system. To accomplish these titrations, $\mathbf{U^{V}O_2}$ was produced by stoichiometric reduction of $\mathbf{U^{VI}O_2}$ with Cp^*_2Co, resulting in a solution of the reduced complex in the cuvette for our studies at a concentration of 100 μM.[35,49] Isosbestic behavior was observed upon the earliest additions of **BA** with (virtually) isosbestic points present in the data at λ_{iso} = 346 nm, 414 nm, and 533 nm and a uniform shift in the peak maximum of the major CT transition to a higher energy (3.32 eV in the profile of $\mathbf{U^{V}O_2}$ to 3.51 eV after the addition of 1 equivalent of **BA**; see SI, Figure S68). Similarly, when between 1 and 2 equivalents of **BA** were added in the spectrochemical titration, the spectral changes remain virtually isosbestic at 414 nm and 533 nm with the peak maximum for the major CT transition experiencing a minute shift to a higher energy from 3.51 eV to 3.55 eV (see SI, Figure S69). Thus, at a [U] = 100 μM, the reactivity of $\mathbf{U^{V}O_2}$ with **BA** appears to be selective on the basis of spectroscopy.

However, NMR spectra collected on reactions conducted at bulk scale with [U] = 4–6 mM involving a 1:1 mixture of $\mathbf{U^{V}O_2}$ and **BA** were consistent with unselective reactivity, in that they display multiple paramagnetically shifted peaks in addition to diamagnetic features corresponding to $\mathbf{U^{VI}O_2}$. We anticipate that the portion of $\mathbf{U^{VI}O_2}$ complex is likely generated by disproportionation reactions of reduced U–**BCF** species since $\mathbf{U^{V}O_2}$ is stable on the time-scale of at least 24 hours in CH_3CN.[35] Similarly, the ^{1}H NMR spectrum of a reaction of $\mathbf{U^{V}O_2}$ with 2 equivalents of **BA** conducted at [U] = 4–6 mM revealed paramagnetically shifted resonances in addition to the diamagnetic resonances of the $\mathbf{U^{VI}O_2}$ complex (see SI, Figure S21). The ^{19}F NMR

spectrum of this reaction shows a veritable "forest" of resonances, including some corresponding to **BA** and some that resemble those measured in prior work[77] on oxygen-bound borane species on the basis of similar chemical shift values (see SI, Figure S22). Based on the use of necessarily higher concentrations in the synthetic work compared to the spectroscopic studies, we hypothesize that **BCF** does likely engages with the oxo moieties of [UO_2^+] to form both 1:1 and 1:2 adducts. However, these species appear to be subject to significant disproportionation reactivity at elevated concentrations, and no diffraction-quality crystals of uranium-containing products were obtained over multiple attempts in this work.[82,83] This observation is in accord with findings from our prior study on reactivity with triphenylborane.[35]

Tying the electrochemical and chemical work conducted in acetonitrile together, we note that the observation of paramagnetically shifted resonances in ^{1}H NMR spectra of reactions of $\mathbf{U^{V}O_2}$ with **BA** in CD_3CN in addition to the observation of very positive oxidative current in the electrochemical titration of $\mathbf{U^{VI}O_2}$ with **BA** in $CH_3CN/TBAPF_6$ suggests that, upon reduction, inner-sphere reactivity likely occurs between **BCF** and the terminal oxo ligands of $\mathbf{U^{V}O_2}$. The resulting reduced, functionalized species may engage in further reactivity, including disproportionation. In particular, the propensity toward disproportionation is supported by observation of selective reactivity (with isosbestic spectral changes) at [U] = 0.1 mM but complex mixtures of products at [U] = 4–6 mM.

Reactivity of U(VI), BCF, and Cp*$_2$Co in CH_2Cl_2. We also explored the reactivity of $\mathbf{U^{VI}O_2}$ with **BCF** in a non-coordinating CH_2Cl_2 solvent, despite the previously established undesirable reactivity of Cp*$_2$Co with CH_2Cl_2 and **BCF**. We did so because of the possibility that Cp*$_2$Co could display faster electron transfer kinetics to uranium complexes in light of the fast electron transfer behavior for $\mathbf{U^{VI}O_2}$ in the cyclic voltammetry studies. Unfortunately, interrogation of the

reaction of $\mathbf{U^{VI}O_2}$ with **BCF** followed by additions of Cp^*_2Co in CH_2Cl_2 through UV-visible detection showed non-isosbestic behavior implicating unselective reactivity (see SI, Figure S72). This is in accord with the previously identified cross-reactivity pathways that can operate between Cp^*_2Co and CH_2Cl_2 and Cp^*_2Co and **BCF**. The high concentration of solvent present under our accessible conditions could give the solvent reactivity an outside role here, as shown in our prior work.[49]

Synthetic-scale work at higher concentrations (4-6 mM) resulted the apparent formation of multiple species as judged by ^{1}H NMR spectroscopy. Fewer paramagnetically shifted peaks were observed in the ^{1}H NMR spectrum of the reaction sequence {$\mathbf{U^{VI}O_2}$ + 1 equiv. **BCF**, followed by 1 equiv. of Cp^*_2Co in CD_2Cl_2} compared to the analogous reaction sequence in CH_3CN {$\mathbf{U^{VI}O_2}$ + 1 equiv. Cp^*_2Co, followed by 1 equiv. of **BA**}. In both cases, however, the distinctive resonances associated with diamagnetic $\mathbf{U^{VI}O_2}$ were detectable, implicating possible roles for disproportionation, as well as incomplete reduction in the case of work in CD_2Cl_2 (see SI, Figure S43). The ^{19}F NMR spectrum of the reaction sequence in CD_2Cl_2 indicates that the **BCF**-containing specie(s) present in the mixture are more shielded, and thus more electron rich, than the **BCF** starting material. This is supported by the measured upfield shift of key resonances and the agreement of the chemical shift values to those associated with similar oxygen-bound **BCF** adducts (see SI, Figure S44).[77] Similarly, the ^{1}H NMR spectrum of the reaction of $\mathbf{U^{VI}O_2}$ with 2 equivalents of **BCF** followed by the addition of Cp^*_2Co reveals the presence of $\mathbf{U^{VI}O_2}$ as well as nine paramagnetically shifted peaks; the ^{19}F NMR spectrum shows shielded (electron rich) **BCF**-containing species as well (see SI, Figures S45 and S46). Taking all of this into account, the reactivity observed here for $\mathbf{U^{VI}O_2}$ with **BCF** and Cp^*_2Co in both coordinating and non-coordinating solvent is outlined in Scheme 5.

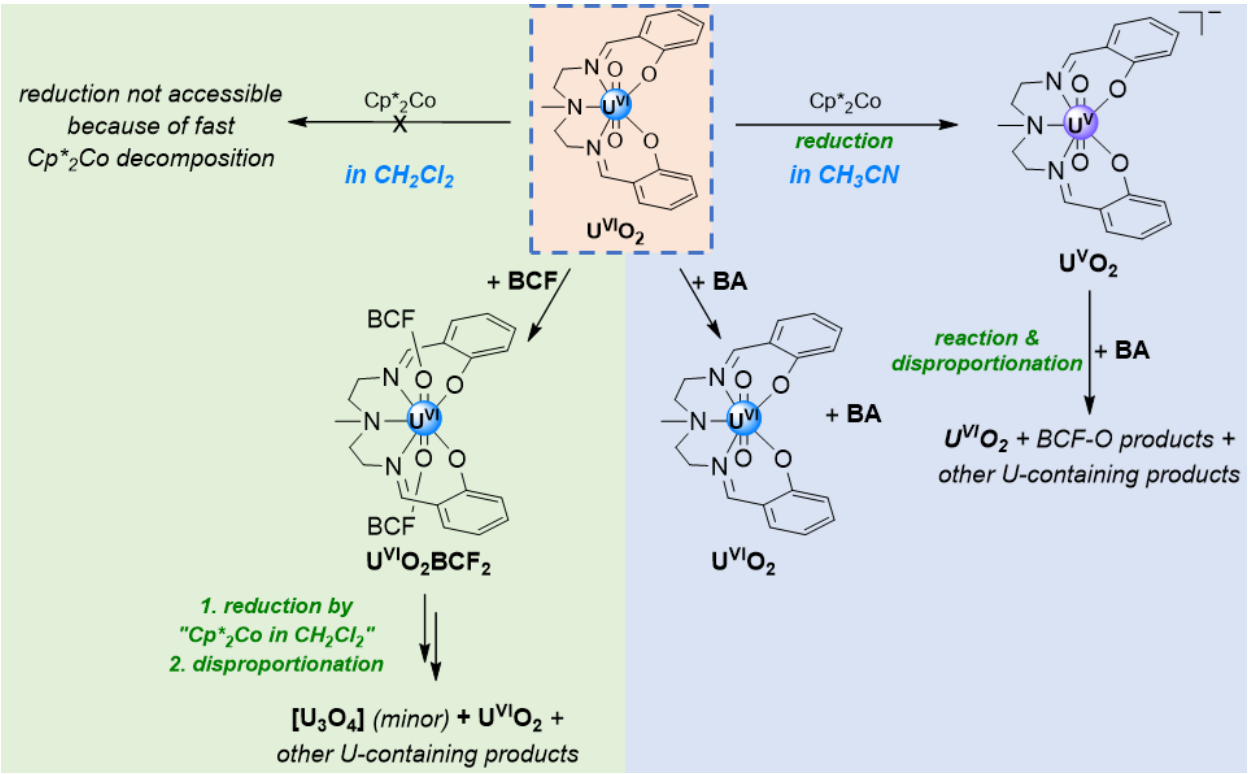

Scheme 5. Summary of reactivity and disproportionation behaviors between $\mathbf{U^{VI}O_2}$ and the reagents employed here in CH_2Cl_2 (left) and CH_3CN (right) as supported by data from spectroscopic, chemical and electrochemical studies.

Structural Characterization of an Oxo-deficient Uranium Species Obtained by Reduction of a Uranyl(VI) Precursor. On one occasion, single crystals of a species denoted **[U_3O_4]** suitable for XRD analysis were grown by vapor diffusion of diethyl ether into a concentrated reaction mixture in CH_2Cl_2. The reaction mixture was prepared according to the following sequence: $\mathbf{U^{VI}O_2}$ was mixed with 2 equiv. **BCF** in CH_2Cl_2, followed by the addition of 1 equiv. of Cp^*_2Co in CH_2Cl_2. The demonstrated ability of **BCF** to associate with $\mathbf{U^{VI}O_2}$ in CH_2Cl_2 led us to conjecture that this sequence might enable BCF-bound uranium-containing species to undergo reduction by Cp^*_2Co or cobalt-containing products of reactivity of Cp^*_2Co with CH_2Cl_2.[49] Indeed, we were able to crystallize such a product (denoted **[U_3O_4]**), although we

emphasize that a crystal of this product was obtained only on one occasion; we anticipate this was the case because of the sensitive and highly activated nature of **[U_3O_4]**. Further, in line with the view of the chemistry of this system demonstrated by the chemical and electrochemical experiments described in this report, the reactions leading to generation of **[U_3O_4]** cannot be considered selective. One such reactivity pathway that could lead to the formation of **[U_3O_4]** involves disproportionation of $\mathbf{U^VO_2}$ to yield a transient $[U^{IV}L]^{2+}$ species, which could then engage in "cation-cation interactions" with remaining $\mathbf{U^VO_2}$ species in a 1:2 fashion to form **[U_3O_4]**. In this pathway, **BCF** could serve to remove the oxos in the disproportionation pathway to form $[U^{IV}L]^{2+}$ in a similar manner as protons in disproportionation pathways in aqueous media. **[U_3O_4]** may not represent the major product of the reactivity obtained with the sequence that was utilized.

Nonetheless, in this case, the species that could be characterized by diffraction studies, **[U_3O_4]**, represents a species of uncommon scholarly interest. One unique feature of this species is that it was formed by reduction-induced uranyl activation and U–O bond cleavage. As demonstrated by the chemical and electrochemical studies reported here, this sort of reactivity remains challenging to control and few examples are available of products produced in this way. As the diffraction data and refined structural model (see Figure 6) were found to be unambiguous, and indeed, of a rather high quality, the structure of **[U_3O_4]** has been included in this work for discussion and computational modelling has been carried out on a limited scale to better understand the properties of this species.

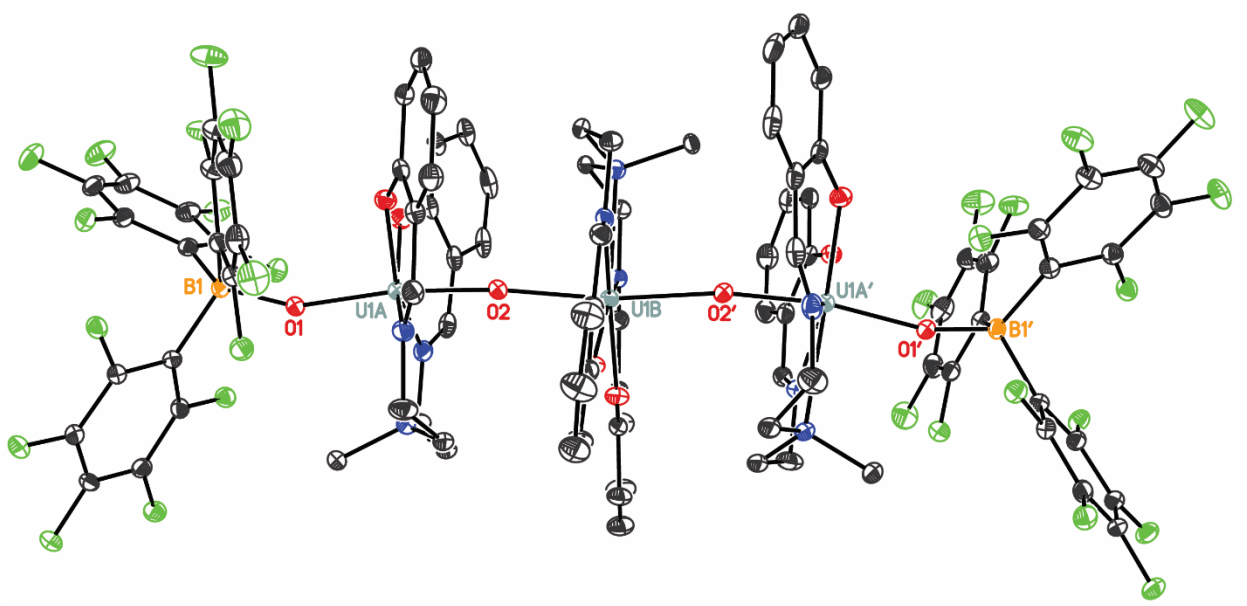

Figure 6. Solid-state structure (XRD) of **[U_3O_4].** All hydrogen atoms, co-crystallized outer-sphere solvent molecules, and disordered atoms associated with the chelating ligands are omitted for clarity. Displacement ellipsoids are shown at the 20% probability level.

Experimental details regarding the crystallography can be found in the Supporting Information (pp. S62–S71 and Table S5). The structure of the crystalline product revealed an oxo-deficient and linear trinuclear uranium core. This core features an uncommon U:O_{oxo} ratio of 3:4, rather than the ratio of 3:6 expected for conventional species with stoichiometry based on multiples of the uranyl motif (U:O_{oxo}, 1:2). Each uranium center is supported by a complete, pentadentate chelating ligand, as well. The asymmetric unit of the structure corresponds to exactly half of the molecular product, and features one **BCF** (B1) bound to one intact uranyl(VI)-derived moiety (U1A) as well as a half-occupied U atom at the center of the linear core motif (U1B). The noted central atom (U1B) is located along a two-fold rotation axis (approximately perpendicular to the axis along which the trinuclear core of the complex lies), with the result that the full trinuclear species can by visualized by rotation about the two-fold axis. Generally speaking, the uranium

atoms are in close proximity to each other with interatomic U1A•••U1B distances of 4.179(1) Å (see Table 1). However, these U–O–U contacts cannot be considered as conventional "cation-cation" interactions between intact actinyl cations (of the Sullivan type[84]) due to the observed deviation from 1:2 U:O_{oxo} stoichiometry.[1,85,86] We note that, at this range, magnetic interactions could occur between unpaired spins on the individual U centers[87,88,89] and these were investigated with quantum chemical calculations. A series of calculations were performed with different spin multiplicities (*vide infra*); the quintet multiplicity yielded the lowest energy and it was used for our subsequent analysis.

With regard to the organic ligand backbone structures, those which chelate the outer uranium centers appear more distorted compared to that chelating the inner uranium center as quantified by the organic ligand fold angles (denoted χ) of 138.7(2)º about U1A and 173.1(4)º about U1B.[90,91] (χ is the angle between the centroid of the mean plane of the carbon atoms composing each aromatic ring of a ligand backbone, two per U–ligand moiety, with the center point of the angle being a point on a plane normal to and centered on a line connecting the centroids of the two previously defined planes.) The extent of folding for the outer ligand appears to be driven by a series of noncovalent π interactions wherein the imine carbon interacts with a phenyl ring (see SI, Figure S103). Two such interactions bend the outer ligand motif towards the inner ligand through interactions between C14A and the phenyl ring composed of C2B–C7B and between C1B and the ring composed of C8A–C13A, with an inter-ring angle of 20.0(3)º. A third interaction between the imine carbon of the outer ligand (C14A) and a ring on the **BCF** moiety (containing C1–C6) causes the rings to be nearly parallel with an inter-ring angle of 7.9(1)º. Finally, weak electrostatic interactions between the fluorine atoms of the **BCF** moiety and the outer organic ligand influence the orientation of the phenyl rings about B1 as well (see SI, Figure S100–S102).

Table 1. Comparison of selected structural parameters of **[U_3O_4]** from X-ray diffraction analysis and DFT calculations for the quintet spin state. Additionally, computed **[U_3O_4]$^-$** at sextet spin state are also presented. ΔR denotes the difference between calculated and observed values.

	[U_3O_4]			**[U_3O_4]$^-$**	
	XRD	**DFT**	ΔR	**DFT**	ΔR
U1A•••U1B (Å)	4.179(1)	4.182	0.003	4.183	0.004
BVS U1A	4.9	-	-	-	-
BVS U1B	3.8	-	-	-	-
U1A–O1A$_{phenoxide}$ (Å)	2.179(4)	2.181	0.002	2.190	0.011
U1A–O2A$_{phenoxide}$ (Å)	2.163(4)	2.172	0.009	2.139	–0.024
U1A–O$_{phenoxide}$ (avg) (Å)	2.171(4)	2.177	0.006	2.165	–0.006
U1A–O1$_{outer\ oxo}$ (Å)	1.994(4)	1.982	–0.012	2.012	0.018
U1A–O2$_{inner\ oxo}$ (Å)	1.976(4)	1.981	0.005	1.995	0.019
U1A–O$_{oxo}$ (avg) (Å)	1.985(4)	1.981	–0.004	1.984	–0.001
O1$_{outer}$–U1A–O2$_{inner}$ (deg)	170.9(2)	173.4	2.5	169.7	–1.2
U1B–O1B$_{phenoxide}$ (Å)	2.192(4)	2.177	–0.015	2.204	0.012
U1B–O2$_{inner\ oxo}$ (Å)	2.220(4)	2.206	–0.014	2.230	0.010
O2$_{inner}$–U1B–O2$_{inner}$ (deg)	172.2(2)	176.9	4.7	174.1	1.9
N1A–C1A (Å)	1.288(9)	1.315	0.027	1.428	0.140
N2A–C14A (Å)	1.272(9)	1.286	0.014	1.278	0.006
N1B–C1B (Å)	1.297(8)	1.284	–0.013	1.447	0.150
B1–O1$_{outer}$ (Å)	1.499(7)	1.538	0.039	1.575	0.076

The U1A–O_{oxo} bond distances and O_{oxo}–U1A–O_{oxo} angles are 1.994(4)/1.976(4) Å and 170.9(2)º for the outer uranium centers, while the inner U1B–O_{oxo} distances are longer at 2.220(4) Å with an O_{oxo}–U1B–O_{oxo} angle (spanning the two-fold rotation axis for the central uranium atom U1B) of 172.2(2)º. The bond metrics for the outer uranium centers are in good agreement with those from literature reports of [U^VO_2] species supported by boranes.[19,35] The uranium atom U1A and its symmetry-generated analogue U1A′ have computed bond valence sum (BVS) values of 4.9, in line with assignment of the formal U(V) oxidation state for the outer U atoms (see Table 1).[19,35,92] The structural data for the inner uranium center (U1B) result in a computed BVS of 3.8, in line with assignment of the formal U(IV) oxidation state for this atom. These formal oxidation

state assignments are supported by the results of computational studies as well (*vide infra*). The U1B–O_{oxo} distances are also consistent with a formal U(IV) O. S. based on the reasonable agreement to literature examples of U(IV) complexes ligated by anionic oxygens.[19,92,93] The metrical data obtained from the structure of **[U_3O_4]** are thus in accord with assignment of this compound as featuring a linear [O–U^V–O–U^{IV}–O–U^V–O] core motif.

Both [U^VO_2] equivalents in **[U_3O_4]** are capped by **BCF** molecules that are engaged in Lewis acid-base interactions with the outer oxo moieties of the linear trinuclear core motif. These boranes show a virtually tetrahedral geometry about boron (B1) on the basis of the calculated τ_4 geometry index of 0.93.[94] The net loss of two oxo moieties from the three total uranium atoms contained within **[U_3O_4]** likely occurs via oxo abstraction from reduced uranyl species by BCF. This conclusion is based on the observation that the U–O bonds of **$U^{VI}O_2$** remained intact according to all chemical and electrochemical tests, except the one case where the powerful combination of CH_2Cl_2 as solvent, Cp^*_2Co as reductant, and BCF as electrophile were utilized. The observation of the uniquely effectiveness of this combination of reagents is reminiscent of the finding of generation of $[OBPh_3]^-$ by oxo abstraction from uranyl species by BPh_3 in a portion of our prior work.[35,95] An alternative hypothesis for the chemical mechanism underlying U–O bond cleavage in this system could involve adventitious water present under the reaction conditions; this possibility is worthy of further exploration as well.

Considering the noted oxo-deficient nature of **[U_3O_4]** that must result in this system from oxo abstraction, we emphasize here that conventional "cation-cation" interactions (CCIs) of the Sullivan type[84] are not present in this structure. CCIs are customarily considered to form between intact actinyl species with 2:1 O_{oxo}:An stoichiometry (or intact actinyls and other metal cations). However, the structure of **[U_3O_4]** does enable observation of a unique interaction between U(V)

and U(IV) via oxo bridges. While T-shaped CCIs of the type $[U^{V}O_2^{+}]$•••$[U^{V}O_2^{+}]$ and interactions involving formation of diamond cores are often observed in complexes containing reduced uranium, bridging oxo interactions between U(V) with U(IV) are much more uncommon.[19,84,85,86] In one example from Mazzanti and co-workers, a tetranuclear complex of mixed valent U(V) and U(IV) denoted here as **$[(U^{V}O_2L)_2(U^{IV}L)_2]$** was reportedly synthesized in a targeted fashion from the reaction of a U(V) precursor complex with $UI_4(Et_2O)_2$ and the potassium salt of an organic chelating ligand.[93] However, unlike the noted prior work that yielded the tetrameric complex, the conditions utilized here were found to be effective for generation of the multimetallic mixed-valent U(V/IV) species denoted **$[U_3O_4]$** solely from a uranyl(VI) starting material using multicomponent reactivity. This route utilized delivery of reducing equivalents and exogeneous electrophiles to uranyl(VI) for oxo activation and abstraction. Thus, the structure of **$[U_3O_4]$** highlights the potency of the reagents employed in the noted test conditions and provides confirmation that multicomponent reactivity can be productive, even if selectivity remains an unmet challenge.

Computational Studies. To gain additional insight into the properties of **$[U_3O_4]$**, the structure obtained from single-crystal XRD was optimized. Using density functional theory (DFT), we analyzed the neutral species **$[U_3O_4]$** and also explored of a hypothetical form of the complex resulting from one-electron reduction, **$[U_3O_4]^{-}$**, to interrogate possible origins of some experimental observations (see Computational Details). Based on the coordination of **$[U_3O_4]$** discussed above, each of the outer uranium (V) ions have one unpaired electron, while the central uranium (IV) possesses two unpaired electrons in their 5f orbitals. Therefore, highest possible spin state was assumed to be $S = 2$ for the neutral and $S = 5/2$ for the anionic structure. The calculated geometric parameters for **$[U_3O_4]$** are compared to those from XRD in Table 1, indicating an excellent agreement with an average difference of approximately 0.011 Å for a neutral complex.

This confirms that the chosen theoretical approach is suitable for reproducing the properties of the complexes.

The geometry optimization of neutral **[U_3O_4]** structure reveals that the U1A–O_{oxo} bond lengths are on average 1.981 Å, while the U1B–$O2_{oxo}$ distance is found to be 2.220 Å. Overall, these are consistent with the oxidation state of U1A (formally U^{V}) and the U1B (formally U^{IV}). [1,19,35] Upon reduction by $1e^{-}$, only minimal changes in the geometry parameters are observed. For instance, **[U_3O_4]$^{-}$** features U–O_{oxo} bonds that are shortened by approximately 0.01–0.04 Å, leading to slightly smaller O_{oxo}–U1A–O_{oxo} angle compared to neutral complex (173.4º vs. 169.7º). This suggests little involvement of metal-centered reduction.

The highest occupied molecular orbitals (HOMO) of **[U_3O_4]** are composed of hybridized 5f orbitals surrounding mainly U1B, while the lowest unoccupied molecular orbitals (LUMOs) surround all uranium atoms, also featuring orbitals resembling mixture of 5f (Figure 7). In **[U_3O_4]$^{-}$**, the HOMO is shifted towards U1A′, while the LUMO is shifted towards U1A. Furthermore, the appearance of HOMO-1 and HOMO-2 suggest electron gain in the ligand (see Figures S89-S90). The reduction process further impacts the HOMO and LUMO energy levels. As calculated the HOMO-LUMO energy gap in the neutral structure is 2.9 eV, while in the reduced species, the gap decreases to 2.1 eV. This change in energy gap levels indicates a decrease the stability of the system, which is in line with the observed non-selective reduction chemistry that resulted from mixing of **$U^{VI}O_2$** and reductants.[16,17,18,19,20,22]

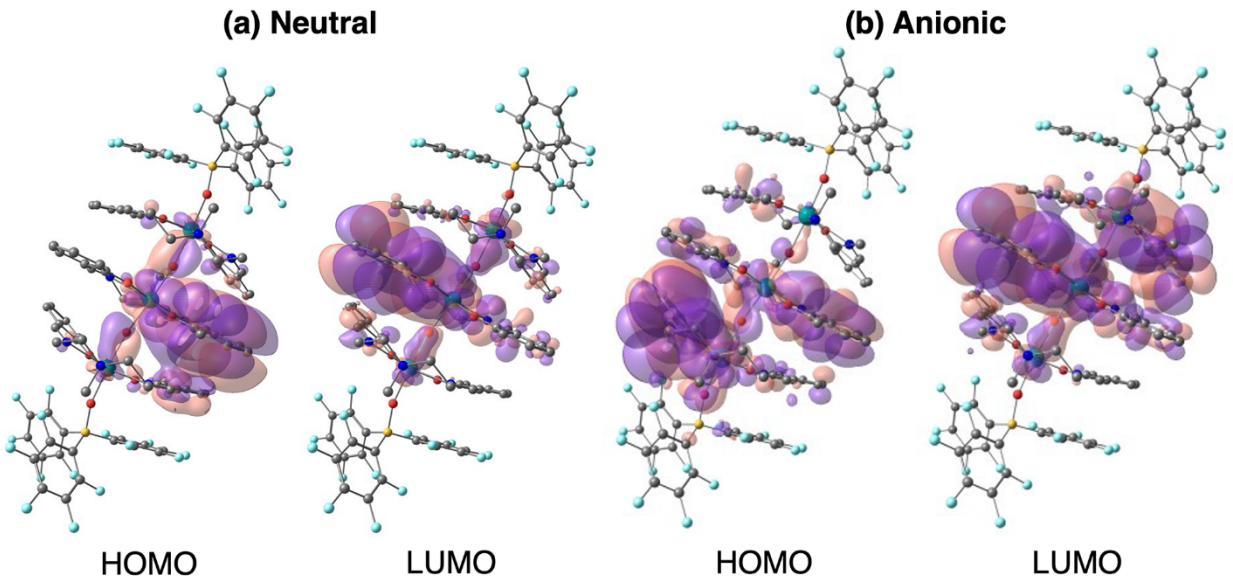

Figure 7. HOMO and LUMO of (a) **[U_3O_4]** (left) and (b) **[U_3O_4]**$^-$ (right). All hydrogen atoms omitted for clarity. Isosurface value of 0.005.

For a deeper understanding of the bonding, natural bond orbital (NBO) analysis was employed as a tool for interpreting chemical bonding and electron density transfer between atoms.[96] This analysis involves examining charge transfer using second-order perturbation analysis of the Fock matrix between filled orbitals of one subsystem and vacant orbitals of another to determine the strength of the interaction energies.[97] As shown in Figure 8 (left structure), the localized orbitals of U1A in **[U_3O_4]** exhibit $5f_{xz^2}$ character, which contribute to the σ-bonding with $O1_{oxo}$ and $O2_{oxo}$. Specifically, there is a significant donation from U1A–O1 to the anti-bonding of U1A–O2, with interaction energies of 0.4 eV. According to natural charges derived from NBO analysis (Table 2), the U1B has a higher charge than U1A (+2.282 vs. +2.140 |e|). Additionally, the $O2_{oxo}$ atom carries more negative charge compared to $O1_{oxo}$, suggesting that the interaction with a highly electrophilic U1B results in weaker bonds between U1B and $O2_{oxo}$ than are often observed in other actinyl compounds.[17,18,19,20,22] This aligns with the observation that the $5f_{yz^2}$ orbitals of U1B show less

involvement in the U1B–$O2_{oxo}$ bond, as indicated by the more modest interaction energy of 0.2 eV (see Table S3).

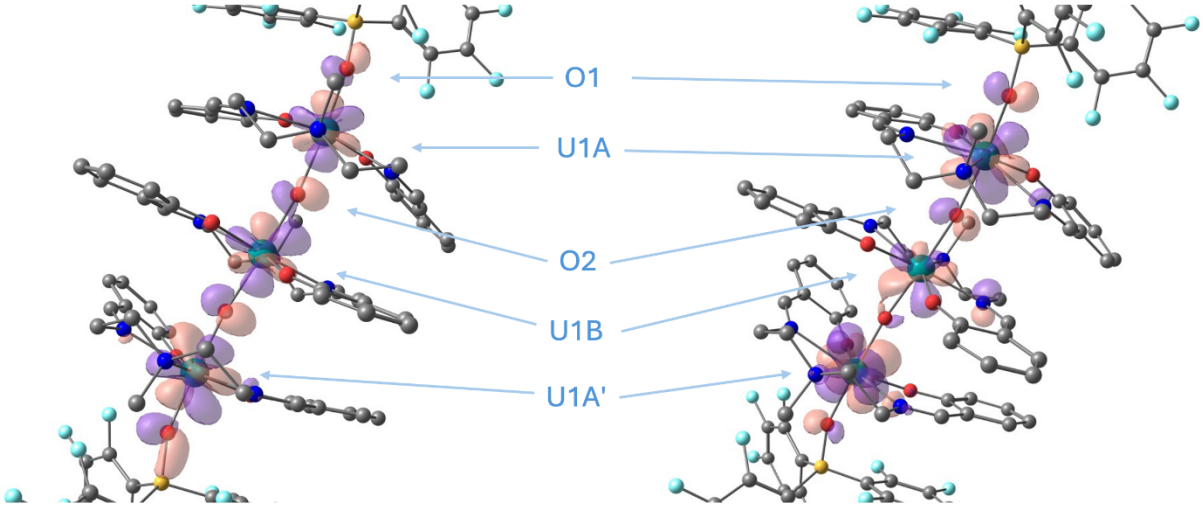

Figure 8. Cut-away views of selected NBOs of **$[U_3O_4]$** (left, NBO 683α) and **$[U_3O_4]^-$** (right, NBO 684α) associated with U–O bonding in the trinuclear core of the structure, with isosurface value of 0.025. All hydrogen atoms omitted for clarity.

Table 2. Comparison of selected natural charges for the neutral and anionic forms of **$[U_3O_4]$**.

Atom	$[U_3O_4]$	$[U_3O_4]^-$	Δ
B1	0.721	0.724	–0.003
$O1_{outer\ oxo}$	–0.894	–0.912	0.018
U1A	2.140	2.107	0.033
$O2_{inner\ oxo}$	–0.981	–0.978	–0.003
$O1A_{phenoxide}$	–0.751	–0.753	0.002
$O2A_{phenoxide}$	–0.749	–0.753	0.004
N1A	–0.428	–0.646	0.218
U1B	2.282	2.291	–0.009
$O1B_{phenoxide}$	–0.776	–0.774	–0.002

Upon the reduction to the **[U$_3$O$_4$]**$^-$ species, the U1A exhibits $5f_{xyz}$ character, with the electron density shifting towards U1A–O1$_{oxo}$ bond (see Figure 8, right structure) making this bond slightly elongated in comparison to in **[U$_3$O$_4$].** Additionally, this bond displays a higher interaction energy of 0.5 eV, contrasting with the 0.3 eV observed in the inner U1A– O2$_{oxo}$ bond. This aligns with an increase in spin density at the U1A atom and decrease at the N1A atoms. Consequently, the N1A atom decreases its natural charges and elongate of the N1A-C1A bond, indicating electron gain in that region (see Table S1-S2). Overall, the computational results suggest that the reactivity of **[U$_3$O$_4$]** can be promoted by ligand-centered reduction, reminiscent of prior findings from Bart and co-workers[98] as well as reminiscent of our observation of oxidative currents at positive potentials in voltammetry conducted in the course of these studies (Figure 5).

Discussion

Uranyl has long been the focus of investigations targeted at reduction and functionalization of its robust actinyl bonds in an effort to accomplish changes in its oxidation state to thereby control its speciation. Studies of this type have employed a wide range of reductants, Lewis acids, and solvents to induce reactivity and have resulted in the characterization of a variety of molecular complexes of functionalized uranyl in oxidation states below +VI. Despite the many examples of molecular products derived from such conditions, disproportionation remains a mode of reactivity that strongly impacts actinide systems and thus plagues analyses of reaction mechanisms and outcomes. In this work, we have evaluated the effectiveness of applying harsh, but commonly used, reagents in the reductive activation of uranyl(VI) housed in an organic ligand under coordinating and non-coordinating solvation environments. (To the best of our knowledge, no other studies have directly compared such conditions on a level playing field as was done here.)

On the one hand, in acetonitrile (a solvent suitable for electrochemical activation strategies), we found that reaction with **BCF** could be achieved upon reduction of uranium, an outcome bolstered by the redox immunity offered to **BCF** by formation of its adduct with acetonitrile. Following activation, disproportionation reactivity ensued and thus appears to preclude the isolation of any reduced products. On the other hand, the unattenuated Lewis acidity of **BCF** in a non-coordinating environment (CH_2Cl_2) enabled reactivity with the very weakly basic oxos of uranyl(VI), providing an electron-deficient species for reduction; these conditions gave rise to a crystalline product/intermediate that apparently arises from disproportionation reactivity on one occasion. The association of **BCF** and other Lewis acids with the oxos of uranyl(VI) is commonly accepted to occur under conditions where other competing Lewis bases are not present, though evidence of such species is sparse aside from the notable structural and spectroscopic work carried out by Sarsfield and Helliwell.[16] Our spectroscopic evidence for such a **BCF**-coordinated species here thus strengthens the case that intermediates of this type could be prevalent across a variety uranyl complexes and conditions under which uranyl oxo activation is studied, especially in non-coordinating media. As reactivity of **BCF** with common electrolyte anions (especially PF_6^-) impedes the use of **BCF** in electrochemical reductive activation pathways in non-specialty electrolytes, we abstained from investigating electrochemical activation under such conditions. However, work with a chemical reductant in the absence of electrolyte could be more confidently carried out; these efforts enabled investigation of the possible modes of undesirable cross- and side-reactivity. In the course of this work, we found ample evidence spurious cross-reactivity modes between multiple components in our studied mixture(s); the cross-reactivity that we have implicated can realistically be anticipated to impact other systems that use the same or similar mixtures of reagents. Lurking in the background of any functionalization scheme employing

U(VI), Cp^*_2Co, **BCF**, and acetonitrile or dichloromethane, there is a serious risk of undesirable outcomes. These insights into cross-reactivity highlight the many accessible reactivity pathways open to the reagents we have studied reagents; our findings could be of interest in a number of research realms because the reagents that we have studied are ubiquitously used in organometallic chemistry focused on both actinides and transition metals. Therefore, our results emphasize the need to proceed carefully in choosing combinations of reagents for reductive activation studies.

In summary, the results described here may not, at first glance, strike the reader as being associated with an especially promising line of research. Indeed, the concept of developing chemical reactivity schemes that involve simultaneous (or sequential) use of reductants and electrophiles is challenging. However, such chemistry is needed for processing of the actinide elements between oxidation states, especially the important early actinides U, Np, and Pu that display a pronounced bonding preference that favors the actinyl ions. In this context, our observations represent a compendium of insights regarding the possible outcomes from, and strategies for, implementing the state-of-the-art approach to U–O bond functionalization chemistry. Clearly, improvements are needed and this work highlights several of them: electrophiles are needed that are resistant to reduction; solvents are needed that are resistant to redox degradation; reductants are needed that are inexpensive and recyclable; tunable reduction potentials could avoid use of harsh reagents. Approaches to several of these challenges are currently under investigation in our laboratories, including implementation of the concept that ligand design for stabilizing reduced intermediates could afford chemistries that avoid the need for harsh stoichiometric reagents.[99] An additional approach under investigation in collaborative work appears to offer the opportunity of avoiding electrophile cross-reactivity through utilization of the

principles of proton-coupled electron transfer, and this strategy is both showing early signs of effectiveness and applicability to both neptunium and plutonium chemistry.[100,101]

Conclusions

This report has described desirable reactivity and undesirable cross-reactivity that can be at play in a system targeted at oxo-functionalization of the uranyl ion, as well as insights into the processes possible when employing common reagents. Significant cross reactivity has been outlined here, highlighting that care should be taken in the design of strategies for actinyl ion processing. On one occasion, the structure of a product of disproportionation reactivity was identified giving insight into the uranium-based reactivity that can be operational under strongly reducing conditions and in the presence of strong Lewis acids. Computational studies predict that the **[U_3O_4]** species could undergo ligand-centered reduction to a more reactive form, giving insights into the electronic structure of both the observed neutral species and the predicted reduced form. Taken together, this work emphasizes the need for mechanistic insight into oxo-activation strategies for the uranyl ion as well as other actinyl ions.

Experimental Section

General Considerations. All manipulations were carried out in dry N_2-filled gloveboxes (Vacuum Atmospheres Co., Hawthorne, CA, USA) unless otherwise noted. All solvents were of commercial grade and dried over activated alumina using a PPT Glass Contour (Nashua, NH) solvent purification system prior to use, and were stored over molecular sieves. All chemicals were obtained from major commercial suppliers and used as received or after extensive drying. CD_3CN and CD_2Cl_2 for NMR studies were purchased from Cambridge Isotope Laboratories (Tewksbury,

MA, USA) and dried over 3 Å molecular sieves or CaH_2, respectively. $\mathbf{U^{VI}O_2}$ was prepared according to literature procedures.[35] ^{1}H, ^{11}B ^{13}C, ^{19}F, and ^{31}P NMR spectra were collected on 400 or 500 MHz Bruker spectrometers at room temperature and referenced to the residual protio-solvent signal in the case of ^{1}H, ^{11}B, and ^{13}C. ^{19}F and ^{31}P NMR spectra were referenced and reported relative to CCl_3F and H_3PO_4, respectively, as external standards following the recommended scale based on ratios of absolute frequencies (Ξ). Chemical shifts (δ) are reported in units of ppm and coupling constants (J) are reported in Hz. Electronic absorption spectra were collected with an Ocean Optics Flame spectrometer equipped with DH-Mini light source, in a 1 cm path length quartz cuvette. Near-infrared spectra were collected with Shimadzu UV-Vis-NIR spectrophotometer (UV-3600) in a 1 cm path length quartz cuvette. Infrared spectra were collected under an inert atmosphere in a dry N_2-filled gloveboxes (Vacuum Atmospheres Co., Hawthorne, CA, USA). Spectra were collected using a Shimadzu IRSpirit Fourier transform infrared spectrometer equipped with a QATR-S single-reflection attenuated total reflectance ATR accessory and diamond prism plate, as well as accessories for conventional transmission measurements in a cell with KBr windows. Solid-state Raman spectra were collected using a Renishaw in-via confocal Raman microscope with an excitation line of 532 nm. Solid samples were placed on a microscope slide with a concave cavity and covered with a glass coverslip affixed with epoxy. Spectra were collected between Δν 100 and 1350 cm^{-1}. Solution-phase Raman spectra were collected using a Horiba Jobin Yvon LabRAM ARAMIS Raman spectrometer with a computer-controlled stage and an excitation line of 785 nm. Samples were placed in a capillary and collected between Δν 100 and 1350 cm^{-1}.

Caution! Depleted uranium (predominantly ^{238}U) was used in this study. ^{238}U is an α-emitting isotope. All manipulations of uranium-containing materials were conducted using appropriate radiological safety controls.

X-Ray Crystallography. Crystals were mounted using Paratone oil with MiTeGen loops and placed under a nitrogen stream for data collection. Low temperature data (100 K) X-ray data were collected using 0.5°-wide ω- or φ-scans on a Bruker D8 Venture diffractometer with a Photon III CPAD detector equipped with Helios high-brilliance multilayer mirror optics. X-rays were provided by a IμS 3.0 Microfocus Mo sealed tube running at 1.4 mA and 50 kV (Mo Kα = 0.71073 Å). All data manipulations were carried out using the Bruker Apex4 Software Suite.[102,103] The data set was corrected for absorption using multi-scan method by SADABS.[104] The Bruker software package SHELXT was used to solve each structure using intrinsic direct methods phasing.[105] Final stages of weighted full-matrix least-squares refinement were conducted using F_o^2 data with SHELXTL in SHELXle and/or Olex2.[106,107,108]

Computational Details. Geometry parameters and energies of uranium complexs **$[U_3O_4]$** and **$[U_3O_4]^-$** were carried out in the gas phase by employing the Perdew-Burke-Ernzerhof (PBE)[109] functional modified with D3 semi-empirical van der Waals corrections[110] within a Gaussian plane wave hybrid basis set scheme.[111] The double zeta basis set was used to describe the valence electron with the cutoff of 400 Ry, where the Goedecker–Teter–Hutter (GTH) type pseudopotential[112] was applied to describe the effect of core electrons. Geometry parameters were calculated using the CP2K package.[113] The optimized coordinates were then used to perform the single point calculations with PBE0[114] along with segmented all-electron relativistically contracted basis sets and the zeroth-order regular approximation with triple zeta quality (SARC-ZORA-TZVP)[115] for the uranium atoms and ZORA-def2-TZVP[116] for rest of the atoms together with the

SARC/J auxiliary basis set using ORCA ver. 4.1.1.[117] Finally, the Natural Bond Orbital (NBO) analysis with the NBO7 code[118] was also carried out. The visualization of molecular orbitals, the NBOs and spin densities are visualized with Chemcraft.[119]

Electrochemistry. Electrochemical experiments were carried out in a nitrogen-filled glove box. Tetra(n-butylammonium) hexafluorophosphate (Sigma-Aldrich; electrochemical grade) (0.1 M in MeCN or DCM) served as the supporting electrolyte for all experiments. Measurements were made with a Gamry Reference 600 Plus Potentiostat/Galvanostat using a standard three-electrode configuration. The working electrode was the basal plane of highly oriented pyrolytic graphite (HOPG) (GraphiteStore.com, Buffalo Grove, IL; surface area: 0.09 cm2), the counter electrode was a platinum wire (Kurt J. Lesker, Jefferson Hills, PA; 99.99%, 0.5 mm diameter), and a silver wire immersed in electrolyte served as a pseudo-reference electrode (CH Instruments). The reference was separated from the working solution by a Vycor frit (Bioanalytical Systems, Inc.). Ferrocene (Sigma Aldrich; twice-sublimed) was added to the electrolyte solution at the conclusion of each experiment (~1 mM) and the midpoint potential of the ferrocenium/ferrocene couple (denoted as $Fc^{+/0}$) served as an external standard for comparison of the recorded potentials.

Bulk electrolyses were performed in a N_2-filled glovebox (Vacuum Atmospheres Co., Hawthorne, CA, USA) in a custom, three-compartment ("W") cells. The central compartment contained a solution of $\mathbf{U^{VI}O_2}$ (8 mM), the left compartment contained ferrocene (8.2 mM), and the right compartment contained blank electrolyte. The electrolysis performed in CH_3CN utilized 0.1 M $TBAPF_6$ as the supporting electrolyte, while the electrolysis performed in CH_2Cl_2 utilized 0.5 M $TBAPF_6$ as the supporting electrolyte.

Associated Content

Supporting Information. The following files are available free of charge:

NMR spectra, characterization data for the complexes reported here, and detailed information regarding the single-crystal X-ray diffraction analysis (PDF) Cartesian coordinates for the structures from XRD (CIF, XYZ)

Acknowledgements

This work was supported by the U.S. Department of Energy, Office of Science, Office of Basic Energy Sciences through the Early Career Research Program (DE-SC0019169). E.R.M. was supported by a U.S. National Science Foundation Research Traineeship (NRT) at the University of Kansas (DGE-1922649). MZM and VAG were supported by ORNL's Laboratory Directed Research and Development (LDRD) program. This research used resources of the National Energy Research Scientific Computing Center (NERSC), a U.S. Department of Energy Office of Science User Facility located at Lawrence Berkeley National Laboratory, operated under Contract No. DE-AC02-05CH11231, as well as resources of the Compute and Data Environment for Science (CADES) at the Oak Ridge National Laboratory, which is supported by the Office of Science of the U.S. Department of Energy under Contract No. DE-AC05-00OR22725. A preprint reflecting a preliminary version of the findings reported here was posted to a preprint server.[120]

Author Information

Corresponding Authors

James D. Blakemore − Department of Chemistry, University of Kansas, Lawrence, Kansas 66045, United States; orcid.org/0000-0003-4172-7460; Phone: +1 (785) 864-3019; E-mail: blakemore@ku.edu

Vassiliki-Alexandra Glezakou − Chemical Sciences Division, Oak Ridge National Laboratory, Oak Ridge, Tennessee 37830, United States; orcid.org/0000-0001-6028-7021; Email: glezakouva@ornl.gov

Authors

Emily R. Mikeska − Department of Chemistry, University of Kansas, Lawrence, Kansas 66045, United States; orcid.org/0000-0001-5149-0132

Małgorzata Z. Makoś − Chemical Sciences Division, Oak Ridge National Laboratory, Oak Ridge, Tennessee 37830, United States; orcid.org/0000-0002-6015-5608

Grant A. Arehart – Department of Chemistry, University of Kansas, Lawrence, Kansas 66045, United States

References

[1] Cowie, B. E.; Purkis, J. M.; Austin, J.; Love, J. B.; Arnold, P. L. Thermal and Photochemical Reduction and Functionalization Chemistry of the Uranyl Dication, $[U^{VI}O_2]^{2+}$. *Chem. Rev.* **2019**, *119*, 10595–10637.

[2] Faizova, R.; Fadaei-Tirani, F.; Chauvin, A.-S.; Mazzanti, M. Synthesis and Characterization of Water Stable Uranyl(V) Complexes. *Angew. Chem.* **2021**, *133*, 8308–8316.

[3] Natrajan, L. S.; Swinburne, A. N.; Andrews, M. B.; Randall, S.; Heath, S. L. Redox and environmentally relevant aspects of actinide(IV) coordination chemistry. *Coord. Chem. Rev.* **2014**, *266–267*, 171–193.

[4] (a) Sadergaski, L. R.; Stoxen, W.; Hixon, A. E. Uranyl Peroxide Nanocluster (U_{60}) Persistence and Sorption in the Presence of Hematite. *Environ. Sci. Technol.* **2018**, *52*, 3304–3311. (b) You, W.; Peng, W.; Tian, Z.; Zheng, M. Uranium bioremediation with U(VI)-reducing bacteria. *Sci. Total Environ.* **2021**, *798*, 149107. (c) Hua, Y.; Wang, W.; Hu, N.; Gu, T.; Ling, L.; Zhang, W. Enrichment of uranium from wastewater with nanoscale zero-valent iron (nZVI). *Environ. Sci.: Nano.* **2021**, *8*, 666–674.

[5] Bard, A. J.; Parsons, R.; Jordon, J., *Standard Potentials in Aqueous Solution.* M. Dekker: New York, 1985.

[6] Berthet, J.-C.; Nierlich, M.; Ephritikhine, M. Complexes triflates de l'uranium. *C. R. Chim.* **2002**, *5*, 81–87.

[7] Cowie, B. E.; Nichol, G. S.; Love, J. B.; Arnold, P. L. Double uranium oxo cations derived from uranyl by borane or silane reduction. *Chem. Commun.* **2018**, *54*, 3839–3842.

[8] Nocton, G.; Horeglad, P.; Vetere, V.; Pécaut, J.; Dubois, L.; Maldivi, P.; Edelstein N. M.; Mazzanti, M. Synthesis, Structure, and Bonding of Stable Complexes of Pentavalent Uranyl. *J. Am. Chem. Soc.* **2010**, *41*, 3542–3547.

[9] (a) Berthet, J.-C.; Siffredi, G.; Thuéry, Ephritikhine, M. Controlled Chemical Reduction of Uranyl Salts into $UX_4(MeCN)_4$ (X = Cl, Br, I) with Me_3SiX Reagents. *Eur. J. Inorg. Chem.*, **2007**, 4017–4020. (b) Kiernicki, J. J.; Zeller, M. Z.; Bart, S. C. Facile Reductive Silylation of UO_2^{2+} to Uranium(IV) Chloride. *Angew. Chem., Int. Ed.* **2017**, *56*, 1097–1100.

[10] Pedrick, E. A.; Wu, G.; Kaltsoyannis, N.; Hayton, T. W. Reductive silylation of a uranyl dibenzoylmethanate complex: an example of controlled uranyl oxo ligand cleavage. *Chem. Sci.* **2014**, *5*, 3204–3213.

[11] Gordon, G.; Taube, H. The Uranium(V) Catalysed Exchange Reaction Between Uranyl Ion and Water in Perchloric Acid Solution. *J. Inorg. Nucl. Chem.* **1961**, *16*, 272–278.

[12] Arnold, P. L.; Pécharman, A.-F.; Lord, R. M.; Jones, G. M.; Hollis, E.; Nichol, G. S.; Maron, L.; Fang, J.; Davin, T.; Love, J. B. Control of Oxo-Group Functionalization and Reduction of the Uranyl Ion. *Inorg. Chem.* **2015**, *54*, 3702–3710.

[13] Pankhurst, J. R.; Bell, N. L.; Zegke, M.; Platts, L. N.; Lamfsus, C. A.; Maron, L.; Natrajan, L. S.; Sproules, S.; Arnold, P. L.; Love, J. B. Inner-sphere vs. outer-sphere reduction of uranyl supported by a redox-active, donor-expanded dipyrrin. *Chem. Sci.* **2017**, *8*, 108–116.

[14] (a) Warren, J. J.; Tronic, T. A.; Mayer, J. M. Thermochemistry of Proton-Coupled Electron Transfer Reagents and its Implications. *Chem. Rev.* **2010,** *110*, 6961-7001. (b) Moyer, B. A.;

Meyer, T. J. Properties of the oxo/aqua system $(bpy)_2(py)RuO^{2+}/(bpy)_2(py)Ru(OH_2)^{2+}$. *Inorg. Chem.* **1981,** *20*, 436-44.

[15] Mikeska, E.R., Wilson, R.E.; Blakemore, J.D. PCET-driven Reactivity of Neptunyl(VI) Yields Oxo-bridged Np(V) and Np(IV) Species, *Chem. Eur. J.*, **2024**, *Accepted Article*, doi: 10.1002/chem.202402963.

[16] Sarsfield, M. J.; Helliwell, M. Extending the Chemistry of the Uranyl Ion: Lewis Acid Coordination to a U=O Oxygen. *J. Am. Chem. Soc.* **2004**, *126*, 1036–1037.

[17] Hayton, T. W.; Wu, G. Exploring the Effects of Reduction of Lewis Acid Coordination on the U=O Bond of the Uranyl Moiety. *Inorg. Chem.*, **2009**, *48*, 3065–3072.

[18] Schnaars, D. D.; Wu, G.; Hayton, T. W. Reduction of Pentavalent Uranyl to U(IV) Facilitated by Oxo Functionalization. *J. Am. Chem. Soc.* **2009**, *131*, 17532–17533.

[19] Bell, N. L.; Shaw, B.; Arnold, P. L.; Love, J. B. Uranyl to Uranium(IV) Conversion through Manipulation of Axial and Equatorial Ligands. *J. Am. Chem. Soc.* **2018**, *140*, 3378–3384.

[20] Berthet, J.-C.; Siffredi, G.; Thuéry, P.; Ephritikhine, M. Controlled Chemical Reduction of Uranyl Salts into $UX_4(MeCN)_4$ (X = Cl. Br, I) with Me_3SiX Reagents. *Eur. J. Inorg. Chem.* **2007**, 4017–4020.

[21] Arnold, P. L.; Patel, D.; Wilson, C.; Love, J. B. Reduction and selective oxo group silylation of the uranyl dication. *Nature* **2008**, *451*(17), 315–317.

[22] Schnaars, D. D.; Wu, G.; Hayton, T. W. Borane-Mediated Silylation of a Metal–Oxo Ligand. *Inorg. Chem.* **2011**, *50*, 4695–4697.

[23] Pedrick, E. A.; Wu, G.; Kaltsoyannis, N.; Hayton, T. W. Reductive solylation of a uranyl dibenzoylmethanate complex: an example of controlled uranyl oxo ligand cleavage. *Chem. Sci.* **2014**, *5*, 3204–3213.

[24] Coughlin, E.; Bart, S. C. Reductive solylation of uranyl mediated by iminosemiquinone ligands. *Polyhedron* **2019**, *170*, 783–787.

[25] Valerio, L. R.; Hakey, B. M.; Brennessel, W. W.; Matson, E. M. Quantitative U=O bond activation in uranyl complexes *via* silyl radical transfer. *Chem. Commun.* **2022**, *58*, 11244–11247.

[26] Fortier, S.; Hayton, T. W. Oxo ligand functionalization in the uranyl ion (UO_2^{2+}). *Coord. Chem. Rev.* **2010**, *254*, 197–214.

[27] Redmond, M. P.; Cornet, S. M.; Woodall, S. D.; Whittaker, D.; Collison, D.; Helliwell, M.; Natrajan, L. S. Probing the local coordination environment and nuclearity of uranyl(VI) complexes in non-aqueous media by emission spectroscopy. *Dalton Trans.* **2011**, *40*, 3914–3926.

[28] Mikeska, E. R.; Ervin, A. C.; Zhang, K.; Benitez, G. M.; Powell, S. M. R.; Oliver, A. G.; Day, V. W.; Caricato, M.; Comadoll, C. G.; Blakemore, J. D. Evidence for Uranium(VI/V) Redox supported by 2,2′-Bipyridyl-6,6′-dicarboxylate. *Inorg. Chem.* **2023**, *62*, 16131–16148.

[29] Takao, K.; Kato, M.; Takao, S.; Nagasawa, A.; Bernhard, G.; Hennig, C.; Ikeda, Y. Molecular Structure and Electrochemical Behavior of Uranyl(VI) Complex with Pentadentate Schiff Base Ligand: Prevention of Uranyl(V) Cation-Cation Interaction by Fully Chelating Equatorial Coordination Sites. *Inorg. Chem.* **2010**, *49*, 2349–2359.

[30] Mizuoka, K.; Kim, S.-Y.; Hasegawa, M.; Hoshi, T.; Uchiyama, G.; Ikeda, Y. Electrochemical and Spectroelectrochemical Studies on UO_2(saloph)L (saloph = N,N‘-Disalicylidene-o-phenylenediaminate, L = Dimethyl Sulfoxide or N,N-Dimethylformamide). *Inorg. Chem.* **2003,** *42*, 1031-1038.

[31] Mougel, V.; Pécaut, J.; Mazzanti, M. New polynuclear U(IV)-U(V) complexes from U(IV) mediated uranyl(V) disproportionation. *Chem. Commun.* **2012**, *48*, 868–870.

[32] Takeyama, T.; Takao, K. Effects of coordinating heteroatoms on molecular structure, thermodynamic stability and redox behavior of uranyl(VI) complexes with pentadentate Schiff-base ligands. *RSC Adv.* **2022**, *12*, 24260–24268.

[33] Takayama, T.; Tsushima, S.; Takao, K. Effects of Substituents on the Molecular Structure and Redox Behavior of Uranyl(V/VI) Complexes with N_3O_2-Donating Schiff Base Ligands. *Inorg. Chem.* **2021**, *60*, 11435–11449.

[34] (a) Augustin, M.; Kerrinnes, H. J.; Langenbeck, W. Chelates of β,β’ bis(salicylaldimino)diethylamine. *J. Prakt. Chem. (Leipzig)* **1964**, *26*, 130–136. (b) Akhtar, M. N.; McKenzie, E. D.; Paine, R. E.; Smith, A. J. Seven coordinate uranyl compounds of the planar quinquedentate ligand N,N’-disalicylidene-1,5-diamino-3-azapentane. *Inorg. Nucl. Chem. Lett.* **1984**, *5*, 673–677. (c) Fenton, D. E.; Casellato, U.; Vigato, P. A.; Vidali, M. Acyclic and macrocyclic Schiff base complexes of lanthanides and actinides. *Inorg. Chim. Acta* **1984**, *95*, 187–193. (d) Bailey, N. A.; Fenton, D. E.; Phillips, C. A.; Casellato, U.; Tamburini, S.; Vigato, P. A.; Graziani, R. The preparation and crystal structure of a dioxouranium(VI) and of an oxovanadium(IV) complex with a hexadentate, compartmental Schiff base ligand. *Inorg. Chim. Acta* **1984**, *109*, 91–98.

[35] Golwankar, R. G.; Makos, M. Z.; Cajiao, N.; Neidig, M. L.; Oliver, A. G.; Day, C. S.; Day, V. W.; Glezakou, V.-A.; Blakemore, J. D. Activation and Functionalization of the Uranyl Ion by Electrochemical Reduction. *Inorg. Chem.* **2024***, 63,* 24542–24553.

[36] Arnold, P. L.; Pécharman, A.-F.; Hollis, E.; Yahia, A.; Maron, L.; Parsons, S.; Love, J. B. Uranyl oxo activation and functionalization by metal cation coordination. *Nat. Chem.* **2010**, *2*, 1056–1061.

[37] Mougel, V.; Horeglad, P.; Nocton, G.; Pécaut, J.; Mazzanti, M. Cation-Cation Complexes of Pentavalent Uranyl: From Disproportionation Intermediates to Stable Clusters. *Chem. Eur. J.* **2010**, *16*, 14365–14377.

[38] Pedrick, E. A.; Assefa, M. K.; Wakefield, M. E.; Wu, G.; Hayton, T. W. Uranyl coordination by the 14-Membered Macrocyclic Dibenzotetramethyltetraaza[14]annulene. *Inorg. Chem.* **2017**, *56*, 6638–6644.

[39] Jones, G. M.; Arnold, P. L.; Love, J. B. Oxo-Group-14-Element Bond Formation in Binuclear Uranium(V) Packman Complexes. *Chem. Eur. J.* **2013**, *19*, 10287–10294.

[40] Arnold, P. L.; Pécharman, A.-F.; Lord, R. M.; Jones, G. M.; Hollis, E.; Nichol, G. S.; Maron, L.; Fang, J.; Davin, T.; Love, J. B. Control of Oxo-Group Functionalization and Reduction of the Uranyl Ion. *Inorg. Chem.* **2015**, *54*, 3702–3710.

[41] Zegke, M.; Nichol, G. S.; Arnold, P. L.; Love, J. B. Catalytic one-electron reduction of uranyl(VI) to Group 1 uranyl(V) complexes *via* Al(III) coordination. *Chem. Commun.* **2015**, *51*, 5876–5879.

[42] Miyamoto, N.; Ikeda, Y.; Tsukahara, T. Multinuclearn NMR Studies on Lewis Acid–Lewis Base Interactions between Bis(pentafluorophenyl)borinic Acid and Uranyl β-Diketonato Complexes in Toluene. *Inorg. Chem.* **2020**, *59*, 11374–11356.

[43] Faizova, R.; Fadaei-Tirani, F.; Bernier-Latmani, R.; Mazzanti, M. Ligand-Supported Facile Conversion of Uranyl(VI) into Uranium(IV) in Organic and Aqueous Media. *Angew. Chem. Int. Ed.* **2020**, *59*, 6756–6759.

[44] Arnold, P. L.; Patel, D.; Blake, A. J.; Wilson, C.; Love, J. B. Selective Oxo Functionalization of the Uranyl Ion with 3d Metal Cations. *J. Am. Chem. Soc.* **2006**, *128*, 9610–9611.

[45] Chatelain, L.; Pécaut, J.; Tuna, F.; Mazzanti, M. Heterometallic F_2^{II}-U^{V} and Ni_2^{II}-U^{V} Exchange-Coupled Single-Molecule Magnets: Effect of the 3d Ion on the Magnetic Properties. *Chem. Eur. J.* **2015**, *21*, 18038–18042.

[46] Faizova, R.; White, S.; Scopelliti, R.; Mazzanti, M. The effect of iron binding on uranyl(V) stability. *Chem. Sci.* **2018**, *9*, 7520–7527.

[47] Arnold, P. L.; Hollis, E.; Nichol, G. S.; Love, J. B.; Griveau, J.-C.; Caciuffo, R.; Magnani, N.; Maron, L.; Castro, L.; Yahai, A.; Odoh S. O.; Schreckenback, G. Oxo-Functionalization and Reduction of the Uranyl Ion through Lanthanide-Element Bond Homolysis: Synthetic, Structural, and Bonding Analysis of a Series of Singly Reduced Uranyl – Rare Earth $5f^{1}$-$4f^{n}$ Complexes. *J. Am. Chem. Soc.* **2013**, *135*, 3841–3854.

[48] Arnold, P. L.; Dutkiewicz, M. S.; Zegke, M.; Walter, O.; Apostolidis, C.; Hollis, E.; Pécharman, A.-F.; Magnani, N.; Griveau, J.-C.; Colineau, E.; Caciuffo, R.; Zhang, X.; Schreckenbach, G.; Love, J. B. Subtle Interactions and Electron Transfer between U^{III}, Np^{III}, or Pu^{III} and Uranyl Mediated by the Oxo Group. *Angew. Chem. Int. Ed.* **2016**, *55,* 12797–12801.

[49] Mikeska, E. R. and Blakemore, J. D. Evidence for Reactivity of Decamethylcobaltocene with Dichloromethane. *Organometallics* **2023**, *42*, 1444–1447.

[50] Chatelain, L.; Tuna, F.; Pécaut, J.; Mazzanti, M. A zig-zag uranyl(V)-Mn(II) single chain magnet with a high relaxation barrier. *Chem. Commun.* **2015**, *51*, 11309–11312.

[51] Mikeska, E. R.; Wilson, R. E.; Sen, A.; Autschbach, J.: Blakemore, J. D. Preparation of Neptunyl and Plutonyl Acetates to Access Nonaqueous Transuranium Coordination Chemistry. *J. Am. Chem. Soc.* **2024**, *146*, 21509–21524.

[52] Ortu, F.; Randall, S.; Moulding, D. J.; Woodward, A. W.; Kerridge, A.; Meyer, K.; La Pierre, H. S.; Natrajan, L. S. Photoluminescence of Pentavalent Uranyl Amide Complexes. *J. Am. Chem. Soc.* **2021**, *143*, 13184–13194.

[53] Madic, C.; Hobart, D. E.; Begun, G. M. Raman Spectrometric Studies of Actinide(V) and –(VI) Complexes in Aqueous Sodium Carbonate Solution and of Solid Sodium Actinide(V) Carbonate Compounds. *Inorg. Chem.* **1983**, *22*, 1494–1503.

[54] Bharara, M. S.; Heflin, K.; Tonks, S.; Strawbridge, K. L.; Gorden, A. E. V. Hydroxy- and alkoxy-bridged dinuclear uranyl-Schiff base complexes: hydrolysis, transamination and extraction studies. *Dalton Trans.* **2008**, 2966–2973.

[55] Herasymchuk, K.; Chiang, L.; Hayes, C. E.; Brown, M. L.; Ovens, J. S.; Patrick, B. O.; Leznoff, D. B.; Storr, T. Synthesis and electronic structure determination of uranium(VI) ligand radical complexes. *Dalton Trans.* **2016**, *45*, 12578–12586.

[56] Mizuoka, K.; Tsushima, S.; Hasegawa, M.; Hoshi, T.; Ikeda, Y. Electronic Spectra of Pure Uranyl(V) Complexes: Characteristic Absorption Bands Due to a $U^{V}O_2^{+}$ Core in Visible and Near-Infrared Regions. *Inorg. Chem.* **2005**, *44*, 6211–6218.

[57] Graves, C. R.; Scott, B. L.; Morris, D. E.; Kiplinger, J. L. Facile Access to Pentavalent Uranium Organometallics: One-Electron Oxidation of Uranium(IV) Imido Complexes with Copper(I) Salts. *J. Am. Chem. Soc.* **2007,** *129*, 11914-11915.

[58] Schnaars, D. D.; Wu, G.; Hayton, T. W. Silylation of the Uranyl Ion Using $B(C_6F_5)_3$-Activated Et_3SiH. *Inorg. Chem.* **2011,** *50*, 9642-9649.

[59] (a) Rajput, A.; Sharma, A. K.; Barman, S. K.; Koley, D.; Steinert, M.; Mukherjee, R. Neutral, cationic, and anionic low-spin iron(III) complexes stabilized by amidophenolate and iminobenzosemiquinonate radical in N, N, O ligands. *Inorg. Chem.* **2014**, *53*, 36–48. (b) Gautam, R.; Loughrey, J. J.; Astashkin, A. V.; Shearer, J.; Tomat, E. Tripyrrindione as a Redox-Active Ligand: Palladium(II) Coordination in Three Redox States. *Angew. Chem. Int. Ed.* **2015**, *54*, 14894–14897. (c) Elvers, B. J.; Krewald, V.; Schulze, C.; Fischer, C. Reduction induced S-nucleophilicity in mono-dithiolene molybdenum complexes – in situ generation of sulfonium ligands. *Chem. Commun.* **2021**, *57*, 12615–12618. (d) Nguyen, T.; Hannah, T. J.; Piers, W. E.; Gelfand, B. S. Stable, π-conjugated radical anions of boron-nitrogen dihydroindeno[1,2-b]fluorenes. *Can. J. Chem.* **2023**, *101*, 111–117.

[60] Kazakov, I. V.; Lisovenko, A. S.; Shcherbina, N. A.; Kornyakov, I. V.; Gugin, N. Y.; Kondrat'ev, Y. V.; Chernysheva, A. M.; Zavgorodnii, A. S.; Timoshkin, A. Y. Structural and Energetic Features of Group 13 Element Trispentafluorophenyl Complexes with Diethyl Ether. *Eur. J. Inorg. Chem.* **2020**, *47*, 4442–4449.

[61] Lorber, C.; Choukroun, R.; Vendier. Reactivity of $B(C_6F_5)_3$ with Simple Early Transition Metal Alkoxides: Alkoxide-Aryl Exchange, THF Ring-Opening, or Acetonitrile CC Coupling. *Organometallics* **2008**, *27*, 5017–5024.

[62] Tao, X.; Daniliuc, C. G.; Knitsch, R.; Hansen, M. R.; Eckert, H.; Lübbesmeyer, M.; Studer, A.; Kehr, G.; Erker, G. The special role of $B(C_6F_5)_3$ in the single electron reduction of quinones by radicals. *Chem. Sci.* **2018**, *9*, 8011–8018.

[63] Jacobsen, H.; Berke, H.; Döring, S.; Kehr, G.; Erker, G.; Fröhlich, R.; Meyer, O. Lewis Acid Properties of Tris(pentafluorophenyl)borane. Structure and Bonding in L-$B(C_6F_5)_3$ Complexes. *Organometallics* **1999**, *18*, 1724–1735.

[64] Bläsing, K.; Bresien, J.; Labbow, R.; Schulz, A.; Villinger, A. A Dimer of Hydrogen Cyanide Stabilized by a Lewis Acid. *Angew. Chem. Int. Ed.* **2018**, *57*, 9170–9175.

[65] Funaioli, T.; Marchetti, F.; Pampaloni, G.; Zacchini, F. Ligand-interchange reactions between M(IV) (M=Ti, V) oxide bisacetylacetonates and halides of high-valent group 4 and 5 metals. A synthetic and electrochemical study. *Dalton Trans.* **2013**, *42*, 14168–14177.

[66] Kokunov, Y. V.; Ershova, M. M.; Razgonyaeva, G. A. NMR Study of the interaction of tim(II) and antimony(III) fluorides with phosphorous chlorides. *Russ. J. Coord. Chem.* **2002**, *28*, 461–463.

[67] Chen, M.-C.; Roberts, J. A. S.; Marks, T. J. New mononuclear and polynuclear perfluoroarylmetalate cocatalysts for stereospecific olefin polymerization. *Organometallics* **2004**, *23*, 932–935.

[68] Chen, C.-H.; Gabbaï. Fluoride Anion Complexation by a Triptycene-Based Distiborane: Taking Advantage of a Weak but Observable C–H•••F Interaction. *Angew. Chem. Int. Ed.* **2017**, *56*, 1799–1804.

[69] Mandal, D.; Gupta, R.; Jaiswal, A. K.; Young, R. D. Frustrated Lewis-Pair-Mediated Selective Single Fluoride Substitution in Trifluoromethyl Groups. *J. Am. Chem. Soc.* **2020**, *142*, 2572–2578.

[70] Kuprat, M.; Lehmann, M.; Schulz, A.; Villinger, A. Synthesis of pentafluorophenyl silver by means of Lewis acid catalysis: structure of silver solvent complexes. *Organometallics* **2010**, *29*, 1421–1427.

[71] Ashley, A. E.; Herrington, T. J; Wildgoose, G. G.; Zaher, H.; Thompson, A. L; Rees, N. H.; Krämer, T.; O'Hare, D. Separating Electrophilicity and Lewis Acidity: The Synthesis, Characterization, and Electrochemistry of the Electron Deficient Tris(aryl)boranes $B(C_6F_5)_{3-n}(C_6Cl_5)_n$ (n = 1-3). *J. Am. Chem. Soc.* **2011**, *133*, 14727–14740.

[72] Harlan, C. J.; Hascall, T.; Fujita, E.; Norton, J. R. The one-electron oxidation of an azazirconacyclobutene in the presence of $B(C_6F_5)_3$. *J. Am. Chem. Soc.* **1999**, *121*, 7274–7275.

[73] Lawrence, E. J.; Oganesyan, V. S.; Wildgoose, G. G.; Ashley, A. E. Exploring the fate of the tris(pentafluorophenyl)borane radical anion in weakly coordinating solvents. *Dalton Trans.* **2013**, *42*, 782–789.

[74] Normand, A. T.; Richard, P.; Balan, C.; Daniliuc, C. G.; Kehr, G.; Erker, G.; Le Gendre, P. Synthetic Endeavors toward Titanium Based Frustrated Lewis Pairs with Controlled Electronic and Steric Properties. *Organometallics* **2015**, *34*, 2000–2011.

[75] Connelly, N. G.; Geiger, W. E. Chemical redox agents for organometallic chemistry. *Chem. Rev.* **1996**, *96*, 877–910.

[76] Bibal, C.; Santini, C. C.; Chauvin, Y.; Vallée, C.; Olivier-Bourbigou, H. A selective synthesis of hydroxyborate anions as novel anchors for zirconocene catalysts. *Dalton Trans.* **2008**, 2866–2870.

[77] Di Saverio, A.; Focante, F.; Camurati, I.; Resconi, L.; Beringhelli, T.; D'Alfonso, G.; Donghi, D.; Maggioni, D.; Mercandelli, P.; Sironi, A. Oxygen-bridged borate anions from tris(pentafluorophenyl)borane: Synthesis, NMR characterization, and reactivity. *Inorg. Chem.* **2005**, *44*, 5030–5041.

[78] Longobardi, L. E.; Mahdi, T.; Stephan, D. W. $B(C_6F_5)_3$ mediated arene hydrogenation/transannulation of para-methoxyanilines. *Dalton Trans.* **2015**, *44*, 7114–7117.

[79] (a) Savéant, J. M.; Costentin, C. *Elements of Molecular and Biomolecular Electrochemistry, An Electrochemical Approach to Electron Transfer Chemistry*. 2nd ed.; Wiley: Hoboken, NJ, 2019; pp. 616. (b) Costentin, C.; Savéant, J.-M. Concepts and tools for mechanism and selectivity analysis in synthetic organic electrochemistry. *Proc. Natl. Acad. Sci. U. S. A.* **2019**, *116*, 11147−11152.

[80] Also in accord with a rapid reaction between the U(V) form of the complex and **BA**, the peak current associated with the reduction of $\mathbf{U^{VI}O_2}$ diminishes as **BA** is added and the overall appearance of the cathodic wave appears to broaden. This behavior is likely attributable to the influence of the fast follow-up reaction that perturbs the Nernstian behavior of the system. Indeed, we have previously observed broadening of a stoichiometric reduction wave in the

presence of an exogeneous acid with which the redox-active species was reacting in a follow up process. See Figure 8 in reference 81b.

[81] Hopkins, J. A.; Lionetti, D.; Day, V. W.; Blakemore, J. D. Chemical and Electrochemical Properties of [Cp*Rh] Complexes Supported by a Hybrid Phosphine-Imine Ligand. *Organometallics* **2019,** *38*, 1300-1310.

[82] On multiple occasions, dark purple crystals were obtained. Diffraction of these crystals yielded the unit cell and structure of the $(Me_5C_5)_3Co_3(\mu_3\text{-}CH)_2$, a complex previously reported by Smith and Andersen. Details regarding the crystallography of $(Me_5C_5)_3Co_3(\mu_3\text{-}CH)_2$ can be found in the Supporting Information (see pp. S46-S47 as well as Table S5). To the best of our knowledge, this compound has not been prepared under any conditions other than those reported by Smith and Andersen; certainly, observation of $(Me_5C_5)_3Co_3(\mu_3\text{-}CH)_2$ under our conditions in acetonitrile solvent was not anticipated. The susceptibility of Cp^*_2Co to attack at the Cp* ring as implicated in our prior work is in accord with the observation of the Smith/Andersen species, however; generation of ring-activated species apparently disturbs the typical stability of the metallocene motif and could facilitate the dissociation of one cyclopentadienyl ring en route to formation of the tricobalt system.

[83] Smith, M. E.; Andersen, R. A. Preparation of the Paramagnetic Hydrides $(Me_5C_5)_3M_3(\mu_3\text{-}CH)(\mu\text{-}H)$ (M = Ni, Co). *Organometallics* **1996**, *15*, 2680–2682.

[84] Sullivan, J. C.; Hindman, J. C.; Zielen, A. J. Specific Interaction between Np(V) and U(VI) in Aqueous Perchloric Acid Media. *J. Am. Chem. Soc.* **1961**, *83*, 3373–3378.

[85] Krot, N. N.; Grigoriev, M. S. Cation-cation interaction in crystallin actinide compounds. *Russ. Chem. Rev.* **2004**, *73*, 89–100.

[86]Augustine, L. J.; Pyrch, M. M. R.; Kravchuk, D. V.; Williams, J. M.; Mason, S. E.; Forbes, T. Z. Density Functional Theory Guided Investigation of Ligand-Induced Neptunyl-Neptunyl Interactions. *Eur. J. Inorg. Chem.* **2023**, *26*, e202200693.

[87] Li, K.; Rajeshkumar, T.; Zhao, Y.; Wang, T.; Maron, L.; Zhu, C. Temperature induced single-crystal to single-crystal transformation of uranium azide complexes. *Chem. Commun.* **2024**. Doi: 10.1039/D4CC00546E

[88] Liddle, S. T.; Slageren, J. v. *Ch. 10 Actinide Single-Molecule Magnets* in *Lanthanides and Actinides in Molecular Magnetism*. Wiley, 2015; 315–339.

[89] Chen, L.; Zheng, T.; Bao, S.; Zhang, L.; Liu, H.-K.; Zheng, L.; Wang, J.; Wang, T.; Diwu, J.; Chai, Z.; Albrecht-Schmitt, T. E.; Wang, S. A Mixed-Valent Uranium Phosphonate Framework Containing U^{IV}, U^{V}, and U^{VI}. *Chem. Eur. J.* **22**, 11954–11957.

[90] Calligaris, M.; Nardin, G.; Randaccio, L. Structural aspects of metal complexes with some tetradentate Schiff bases. *Coord. Chem. Rev.* **1972**, *7*, 385–403.

[91] Mikeska, E. R.; Lind, N. M.; Ervin, A. C.; Khalife, C.; Karnes, J. P; Blakemore, J. D. Observations regarding the synthesis and redox chemistry of heterobimetallic uranyl complexes containing Group 10 metals. *Radiochim. Acta* **2024**. Doi: /10.1515/ract-2023-0237

[92] Gagne, O. C.; Hawthorne, F. C. Comprehensive derivation of bond-valence parameters for ion pairs involving oxygen. *Acta Crystallogr. Sec. B* **2015**, *71*, 562–578.

[93] Mougel, V.; Pécaut, J.; Mazzanti, M. New polynuclear U(IV)-U(V) complexes from U(IV) mediated uranyl(V) disproportionation. *Chem. Commun.* **2012**, *48*, 868–870.

[94] Yang, L.; Powell, D. R., Houser, R. P. Structural variation in copper(I) complexes with pyridylmethylamide ligands: structural analysis with a new four-coordinate geometry index, τ_4. *Dalton Trans.* **2007**, 955–964.

[95] Mayer, R. J.; Hampel, N.; Ofial, A. R. Lewis Acidic Boranes, Lewis Bases, and Equilibrium Constants: A Reliable Scaffold for a Quantitative Lewis Acidity/Basicity Scale. *Chem. Eur. J.* **2021**, *27*. 4070–4080.

[96] (a) Glendening, E. D.; Badenhoop, J. K.; Reed, A. E.; Carpenter, J. E.; Bohmann, J. A.; Morales, C. M.; Karafiloglou, P.; Landis, C. R.; and Weinhold, F. NBO 7.0., Theoretical Chemistry Institute, University of Wisconsin, Madison, 2018. (b) Suidan, L.; Badenhoop, J. K.; Glendening, E. D.; Weinhold, F. Common Textbook and Teaching Misrepresentations of Lewis Structures. *J. Chem. Ed.* **1995,** *72*, 583. (c) Weinhold, F. Chemical Bonding as a Superposition Phenomenon. *J. Chem. Ed.* **1999,** *76*, 1141.

[97] Weinhold, F.; Landis, C. R. Natural bond orbitals and extensions of localized bonding concepts. *Chem. Educ. Res. Pract.* **2001**, *2*, 91–104.

[98] Kiernicki, J. J.; Cladis, D. P.; Fanwick, P. E.; Zeller, M.; Bart, S. C. Synthesis, Characterization, and Stoichiometric U–O Bond Scission in Uranyl Species Supported by Pyridine(diimine) Ligand Radicals. *J. Am. Chem. Soc.* **2015,** *137*, 11115-11125.

[99] Golwankar, R. R.; Ervin, A. C.; Makoś, M. Z.; Mikeska, E. R.; Glezakou, V.-A.; Blakemore, J. D. Synthesis, Isolation, and Study of Heterobimetallic Uranyl Crown Ether Complexes. *J. Am. Chem. Soc.* **2024,** *146*, 9597-9604.

[100] Mikeska, E.R.; Wilson, R.E.; Blakemore, J.D. PCET-driven Reactivity of Neptunyl(VI) Yields Oxo-bridged Np(V) and Np(IV) Species, *Chem. Eur. J.*, **2024**, *Accepted Article*, doi: 10.1002/chem.202402963.

[101] (a) Mikeska, E.R., Wilson, R.E., Sen, A., Autschbach, J., Blakemore, J.D. Preparation of Neptunyl and Plutonyl Acetates to Access Non-Aqueous Transuranium Coordination Chemistry, *J. Am. Chem. Soc.* **2024**, *146*, 21509-21524. (b) Mikeska, E.R., Curry, T.D., Wilson, R.E., Blakemore, J.D. Electroanalytical Characterization of Np(VI)/Np(V) Redox in a Pentadentate Ligand Environment and Stabilization of $[Np^{V}O_2]^+$ by Hydrogen Bonding, *Dalton Trans.*, **2024**, *53*, 19126-19142.

[102] *APEX-4.* Bruker Analytical X-ray Systems Inc.: Madison, WI, USA, 2022.

[103] *SAINT Ver. 8.40A.* Bruker Analytical X-ray Systems Inc.: Madison, WI, USA, 2022.

[104] Krause, L.; Herbst-Irmer, R.; Sheldrick, G. M.; Stalke, D. Comparison of silver and molybdenum microfocus X-ray sources for single-crystal structure determination. *J. Appl. Crystallogr.* **2015**, *48*, 3–10.

[105] Sheldrick, G. M. SHELXT – Integrated space-group and crystal-structure determination. *Acta Crystallogr., Sect. A: Found. Crystallogr.* **2015**, *71*, 3–8.

[106] Sheldrick, G. M. Crystal structure refinement with SHELXL. *Acta Crystallogr., Sect. C: Struct. Chem.* **2015**, *71*, 3–8.

[107] Hübschle, C. B.; Sheldrick, G. M.; Dittrich, B. ShelXle: a Qt graphical user interface for SHELXL. *J. Appl. Crystallogr.* **2011**, *44*, 1281–1284.

[108] Dolomanov, O. V.; Bourhis, L. J.; Gildea, R. J.; Howard, J. A. K.; Puschmann, H. Olex2: a complete structure solution, refinement, and analysis program. *J. Appl. Crystallogr.* **2009**, *42*, 339–341.
[109] Perdew, J. P.; Burke, K.; Ernzerhof, M., Generalized Gradient Approximation Made Simple. *Phys. Rev. Lett.* **1996**, *77*, 3865–3868.
[110] Grimme, S.; Antony, J.; Ehrlich, S.; Krieg, H. A consistent and accurate *ab initio* parametrization of density functional dispersion correction (DFT-D) for the 94 elements H-Pu. *J. Chem. Phys.* **2010**, *132*, 154104.
[111] Lippert, G.; Hutter, J.; Parrinello, M. A hybrid Gaussian and plane wave density functional scheme. *Mol. Phys.* **1997**, *92*, 477–487.
[112] Goedecker, S.; Teter, M.; Hutter, J. Separable dual-space Gaussian pseudopotentials. *Phys. Rev. B* **1996**, *54*, 1703–1710
[113] VandeVondele, J.; Krack, M.; Mohamed, F.; Parrinello, M.; Chassaing, T.; Hutter, J. Quickstep: Fast and accurate density functional calculations using a mixed Gaussian and plane waves approach. *Comput. Phys. Commun.* **2005**, *167*, 103–128.
[114] Perdew, J. P.; Ernzerhof, M.; Burke, K. Rationale for mixing exact exchange with density functional approximations. *J. Chem. Phys.* **1996**, *105*, 9982–9985.
[115] Pantazis, D. A.; Neese, F. All-Electron Scalar Relativistic Basis Sets for the Actinides. *J. Chem. Theory Comput.* **2011**, *7*, 677–684.
[116] Weigend, F.; Ahlrichs, R. Balanced basis sets of split valence, triple zeta valence and quadruple zeta valence quality for H to Rn: Design and assessment of accuracy. *Phys. Chem. Chem. Phys.* **2005**, 7, 3297–3305.
[117] Neese, F. Software update: the ORCA program system, version 4.0. WIREs Computational. *Mol. Sci.* **2017**, *8*, e1327.
[118] *NBO 7.0.* Glendening, E. D.; Badenhoop, J. K.; Reed, A. E.; Carpenter, J. E.; Bohmann, J. A.; Morales, C. M.; Karafiloglou, P.; Landis, C. R.; Weinhold, F. Theoretical Chemistry Institute, University of Wisconsin, Madison, WI (2018).
[119] Chemcraft – graphical software for visualization of quantum chemistry computations. Version 1.8, build 648.
[120] Mikeska, E., Makos, M., Glezakou, V.-A., Blakemore, J.D. Reactivity and Cross-Reactivity in Redox Activation of the Uranyl Ion, *ChemRxiv (Inorg. Chem.)*, **2024**, doi: 10.26434/chemrxiv-2024-nhgcl.

TOC Graphic

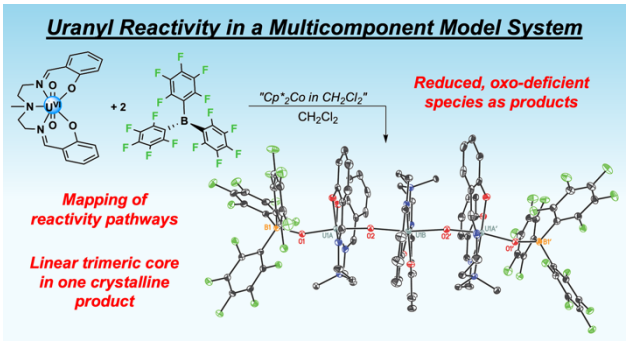

TOC Synopsis

A multicomponent model system for reductive activation and functionalization of the uranyl ion, UO_2^{n+}, has been studied. Reactivity and cross-reactivity pathways have been mapped for the system in two solvents (acetonitrile and dichloromethane) and under both chemical and electrochemical conditions. One crystalline and oxo-deficient product featuring a trimetallic uranium core was characterized, highlighting the usefulness of the reductive activation scheme.